NACA

RESEARCH MEMORANDUM

PERFORMANCE CHARACTERISTICS OF AN UNDERSLUNG

VERTICAL-WEDGE INLET WITH POROUS SUCTION

AT MACH NUMBERS OF 0.63 AND 1.5 TO 2.0

By John L. Allen and Thomas G. Piercy

Lewis Flight Propulsion Laboratory
Cleveland, Ohio

NATIONAL ADVISORY COMMITTEE
FOR AERONAUTICS
WASHINGTON
August 3, 1956

NATIONAL ADVISORY COMMITTEE FOR AERONAUTICS

RESEARCH MEMORANDUM

PERFORMANCE CHARACTERISTICS OF AN UNDERSLUNG VERTICAL-WEDGE INLET

WITH POROUS SUCTION AT MACH NUMBERS OF 0.63 AND 1.5 TO 2.0

By John L. Allen and Thomas G. Piercy

SUMMARY

The performance of a ventrally mounted inlet having a variable-angle vertical-wedge compression surface was determined at Mach numbers of 0.63 and 1.5 to 2.0 for a range of angles of attack, angles of yaw, and wedge angle. A solid wedge and wedges with two different porosities were tested. The variable-angle-wedge mechanical system as well as the systems for ingesting and discharging wedge bleed-air flow or fuselage boundary-layer-removal air flow were typical of those for full-scale airplane application.

The performance obtained with the solid wedge for optimum schedules of wedge angle was improved 3 and 5 percent of ideal engine thrust at Mach numbers of 1.5 and 2.0, respectively, by bleeding 3 to 6 percent of the maximum capture mass flow through the porous wedge. Increasing porosity, and hence bleed flow, progressively increased pressure recovery except at a Mach number of 1.5, where the improvement was about one-half of that at higher Mach numbers. Bleeding air from the hinge system and clearance spaces for the solid wedge and altering the plan form of the splitter plate contributed to performance gains, particularly at Mach numbers greater than 1.5.

Angles of attack between $\pm 4^{\circ}$ had only minor effects; however, angles of yaw of 6° decreased the effective thrust ratio between 10 and 15 percent of ideal thrust. In the yaw condition at subcritical mass flows, regions of asymmetric shock structure on either side of the wedge seriously increased the total-pressure distortion at the compressor inlet.

At engine matching conditions the total-pressure distortion at the compressor-inlet station decreased from 16 to 6 percent between flight Mach numbers of 1.5 and 2.0.

The use of wedge static-pressure orifices to provide an input signal for a normal-shock-positioning control was analyzed. The results indicated that for the zero yaw condition net-thrust-minus-drag could be maintained within 1 percent of the optimum value.

INTRODUCTION

Previous results (refs. 1 and 2) have shown the comparative performance and relative advantages of inlets using a vertical-wedge compression surface. The benefits of using area suction on a porous wedge to remove low-energy air are reported in reference 3. In the present investigation a one-fifth scale model of a forebody of a fighter-type airplane having a ventrally mounted porous-vertical-wedge inlet was tested in the NACA Lewis 8- by 6-foot supersonic wind tunnel. The mechanical design and the porous surface of the variable-angle wedge were typical of those for a full-scale airplane. The systems for bleeding and discharging air from the porous wedge and from ram boundary-layer air scoops between the fuselage and splitter plate were also selected to be representative of a full-scale airplane.

Force and pressure-recovery data were obtained for wedges that were solid, 3.5-percent porous, and 5-percent porous. The wedge angle was varied from 6° to 16°, the angle of attack from -4° to +4°, and the angle of yaw from 0° to 6°. Flight Mach numbers of 0.63 and 1.5 to 2.0 were investigated. The plan form of the splitter plate was varied from triangular to cutback.

An analysis of a shock-positioning device using wedge static pressures for an input signal was made by Fred Wilcox and Norman Musialowski. Inasmuch as this study is considered supplementary to the primary purpose of the report, these results are presented in the appendix.

SYMBOLS

A area, sq ft

A_c inlet capture area, 0.192 sq ft

A_{max} model frontal area, 0.9445 sq ft

A_2 area at compressor inlet, 0.205 sq ft

C_D drag coefficient, $D/q_0 A_{max}$

D drag

F_n engine net thrust

$F_{n,i}$ engine ideal net thrust, 100 percent ram

H total pressure

$\dfrac{\Delta H}{H_{av}}$ total-pressure distortion parameter, numerical difference between maximum and minimum rake total pressures divided by average total pressure, percent

h   boundary-layer splitter height, 0.3 in.

M   Mach number

$\dfrac{m}{m_0}$ mass-flow ratio, $\dfrac{\rho V A}{\rho_0 V_0 A_c}$

$\dfrac{m_i}{m_0}$ inlet mass-flow ratio, $\dfrac{m_2}{m_0} + \dfrac{m_w}{m_0}$

p   static pressure

q   dynamic pressure

V   velocity

w   weight flow, lb/sec

$\dfrac{w\sqrt{\theta}}{\delta A}$ corrected rate of weight flow of air per unit area, lb/(sec)(sq ft)

y   vertical distance from fuselage

α angle of attack, deg

δ ratio of local total pressure to NACA standard sea-level static pressure of 2116 lb/sq ft

θ ratio of total temperature to NACA standard sea-level static temperature of 519° R

ρ mass density of air

σ wedge half-angle, deg

ψ angle of yaw, deg

Subscripts:

i   inlet

l local

r   reference orifice

s   normal-shock-position sensing orifice

w   wedge

0   free stream

1   inlet survey station 22.1

2   compressor inlet, station 87.5

Configuration designations:

S_t triangular-splitter-plate plan form (fig. 3)

S_c cutback-splitter-plate plan form (fig. 3)

P_0 solid-wedge plates

$P_{3.5}$ 3.5-percent-porous-wedge plates

$P_{5.0}$ 5.0-percent-porous-wedge plates

E_0 sealed porous-wedge air exits

E_s small porous-wedge air exits, area = 0.01472 sq ft

E_m medium-sized porous-wedge air exits, area = 0.0296 sq ft

E_l large porous-wedge air exits, area = 0.0441 sq ft

APPARATUS AND PROCEDURE

A schematic drawing of the one-fifth scale model is shown in figure 1, and photographs of the variable-angle, porous-vertical-wedge inlet are presented in figure 2.

The inlet was located on the bottom of the fuselage. A wedge-type diverter was located between the inlet splitter plate and the fuselage. Two scoops located near the aft portion of this diverter furnished air for an auxiliary airplane system. Details of the wedge hinge system and location of porous-wedge surfaces are shown in figure 3 as well as details of the fuselage boundary-layer diverter and air scoops. The two static-pressure taps on the second compression surfaces were used for the controls study presented in the appendix.

Variable-Angle Porous Wedge

The fixed-leading-edge portion of the wedge had a half-angle of $6°$, and the angle of the second wedge was variable from $6°$ to $16°$. Thus, two oblique compression shocks could be generated when desired. Air bled through the porous portion of the wedge passed from the control valve located over the cavity between the sides of the wedge into a reservoir chamber. The air then passed through the metering nozzle into ducts located near the sides of this nozzle and out exits located on the sides of the fuselage (figs. 1 and 2). During the course of testing, additional bleed capacity was needed. Consequently, an additional exit was installed in the top of the wedge reservoir chamber (fig. 1). Air flow through this exit was not measured by the metering nozzle.

Porous plates having 3.5- and 5-percent open area were tested as well as solid or nonporous plates. The porous plates were characterized by uniformly spaced holes on an otherwise smooth surface. Porous plates were installed on the wedge surfaces between stations 27.9 and 35.5, this distance being about 20 percent of the total side area of the wedge. For the 5-percent-porous plates this amounts to about 0.7 percent of the total wedge area. The porous plates were attached to a grid-like rib structure that was carefully constructed to furnish support with a minimum of blockage.

The porous-wedge air-bleed system also removed air from the hinge gaps and from the clearance gaps between the top and bottom of the wedge and inlet duct surface. The relative amount of this air flow was evaluated by testing the solid-wedge configuration P_0 with the wedge bleed exits sealed flush with the external body contour E_0 and then with the small exit area E_s.

Fuselage Boundary-Layer Removal System and Splitter-Plate Plan Form

The wedge-type boundary-layer diverter between the fuselage and inlet splitter plate had a half-angle of about $20°$ (fig. 3). Air captured by the two scoops located near the aft portion of this diverter was ducted through separate metering nozzles to a reservoir chamber which had an exit located on the upper starboard side. The scoop mass flow could be regulated by means of perforated plates that changed the flow area of the exit. Two splitter-plate plan forms were tested. The triangular plate is designated S_t, and the cutback splitter plate, S_c (fig. 3).

Force, Pressure, and Mass-Flow Measurements

The strain-gage balance measured external and base forces back to the fuselage split near station 56 (section E-E, fig. 1). This portion of the model fell within the reflected shock pattern. The balance also measured internal forces back to station 135, where the duct was split. The labyrinth seal reduced leakage at the duct split to an insignificant amount and did not interfere with the force measurements. This portion of the model (stations 56 to 168) was covered by a windshield. The part of the model aft of station 168 consisted of a mass-flow measuring system which included four flow-straightening screens, a calibrated metering nozzle, and a mass-flow control plug. Each of the metering nozzles had four static-pressure taps at both the throat and upstream stations for computing mass flow.

In order to find external drag coefficients, base pressures were measured around the joint formed by the front and rear sections (station 55), in the internal base area (station 55), and at the base of the duct near the labyrinth seal. The force on the duct due to the change in duct cross-sectional area within the windshield was accounted for and subtracted from the force measurements. Static-pressure measurements immediately aft of the duct split (station 136) and continuity of mass flow were used to compute duct-exit momentum. External drag coefficient includes drag due to inlet shock spillage, friction and pressure drag on the inlet and body ahead of station 55, and the porous wedge and boundary-layer-scoop air flows. A faired nose (fig. 1) was also tested so that incremental forces due to the inlet and secondary air systems could be evaluated.

The compressor-inlet station, which was canted 3° up relative to the angle-of-attack axis, had a six-segment rake with six total-pressure tubes per segment spaced for an approximate Gaussian weighting. Average pressure recoveries from this rake were in good agreement with calculations based on static pressure, mass flow, and area. The inner and outermost rings of total-pressure tubes would be about 1/4 inch from the respective surfaces on a full-scale duct. These tubes were used as the flow-profile lower limit for the total-pressure-distortion calculation $\Delta H/H_{av,2}$.

In order to determine the flow field of the inlet, a survey was taken at station 22.1 at the vertical centerline. Instrumented 6° half-angle wedges were installed 3.5 and 1.5 inches from the fuselage for determining the local Mach number, total pressure, and flow direction. The wedge 3.5 inches from the surface was nearly alined with the outermost portion of the cowl lip. Five total-pressure tubes were used to define the boundary-layer profile.

The air flow through the auxiliary top exit, when used, was estimated by assuming choking at a total pressure equal to the reservoir static pressure. By adding this top exit air flow, the metered wedge air flow, and the mass flow leaving the model main duct for supercritical inlet conditions, the mass-flow ratio entering the inlet was found and compared with supercritical mass-flow ratio for similar solid-wedge data. The difference in supercritical inlet mass-flow ratios was then arbitrarily applied as a correction factor for wedge air flows for all inlet operating conditions.

Subsonic-Diffuser Characteristics

The subsonic-diffuser-area variation is shown in figure 4. A large portion of the total area expansion occurred between the inlet lip and the end of the variable-wedge section (station 42.0). However, average equivalent conical diffuser expansion angles between the inlet throat and station 42.0 were only about 1° and 4° for the 6° and 16° wedge positions, respectively.

RESULTS AND DISCUSSION

Inlet Flow-Field Survey

Results of the flow-field survey ahead of the inlet are presented in figure 5. In general, the total-pressure loss ahead of the inlet was less then 1 percent for the region beyond the splitter plate at angles of attack of 0° and 4° and Mach numbers of 1.7 to 2.0. At a Mach number of 1.5, however, this loss was increased slightly for zero angle of attack. The flow profiles became less favorable at negative angles of attack and higher Mach numbers, which is the usual trend for this inlet location. Ahead of the inlet a 0.04 to 0.14 Mach number reduction was obtained, depending on the angle of attack. Although low-energy air appeared to enter the inlet for some conditions, as indicated by the splitter-plate height, these plots are not truly indicative of the amount of low-energy air entering the inlet inasmuch as the splitter-plate height increased outboard of the vertical centerline of the model.

Comparison of Inlet Configurations

A comparison of total-pressure recovery and wedge bleed mass-flow ratios against inlet mass-flow ratio (exit plus bleed mass flow) is presented in figure 6 for Mach numbers of 1.9 and 1.5 for an angle of attack of 2°. For each Mach number three comparisons are shown: (1) triangular splitter-plate inlet having a solid wedge with and without hinge and gap bleed flow and with the 3.5-percent-porous wedge; (2) effect of varying

the splitter plate from triangular to cutback for the solid and 3.5-percent-porous wedges; (3) the cutback-splitter-plate inlet having wedges that are solid, 3.5-percent porous, 5-percent porous, and 5-percent porous with increased exit area. The trends shown for a Mach number of 1.9 are typical for Mach numbers above 1.5 and up to 2.0.

At a Mach number of 1.9 for a wedge angle of 12°, bleeding air from the hinges and clearance gaps increased the total-pressure recovery as much as 3 percent of that for the no-bleed case for a bleed mass flow of about 1 percent of the maximum capture mass-flow ratio. With the 3.5-percent-porous wedge $P_{3.5}$, the pressure recovery was increased as much as 7 percent of that for the no-bleed case for about 3.5-percent bleed flow. However, at a Mach number of 1.5, similar bleed flows resulted in less than one-half of the percentage increase obtained at higher Mach numbers. Because of limited data, the performance shown for the solid 8° wedge is considered typical of that of a 7° wedge with respect to pressure recovery. Changing the splitter-plate plan form from triangular to cutback $(S_t$ to $S_c)$ increased the pressure recovery as much as 2 to $2\frac{1}{2}$ percent and increased the captured mass flow by slightly more than 1 percent for both the solid and porous wedges at a Mach number of 1.9. These effects were practically negligible at a Mach number of 1.5. For the cutback-splitter-plate inlet S_c, increasing the wedge porosity from 3.5 to 5.0 percent had very little effect on pressure recovery, and the wedge bleed flow did not increase very much. Consequently, the bleed exit area was increased from E_m to E_l; and, as a result, the pressure recovery increased slightly more than 1 percent $(S_c P_{5.0} E_m$ to $S_c P_{5.0} E_l)$. Since the wedge bleed flow, which was estimated for $S_c P_{5.0} E_l$ (see APPARATUS AND PROCEDURE), was not increased appreciably, the better pressure recovery may be mainly associated with improved distribution of the bleed flow.

Performance of the $S_c P_{5.0} E_l$ Inlet

The performance of the optimized inlet, characterized by the swept-back splitter plate in combination with maximum bleed, was determined in some detail. The variation of drag coefficient, total-pressure recovery, and percentage of total-pressure distortion with exit mass-flow ratio is presented in figures 7 to 9. The performance is compared with that of the solid or nonporous wedge whenever possible. Typical total-pressure contours at the compressor-inlet station are presented in figure 10. The effects include wedge angle, free-stream Mach number, angle of attack, and angle of yaw. Lines of constant rate of corrected weight flow per unit area are superimposed on figures 7 to 9, and the required engine plus cooling-air values are indicated for a conventional two-spool compressor turbojet engine with afterburner. Drag coefficient values for the faired-nose configuration are indicated on the ordinate.

3979

Effect of Free-Stream Mach Number at Angle of Attack of 2°

A comparison of the porous-wedge inlet with the solid-wedge inlet for the expected cruise angle of attack of 2° is shown in the following table:

Free-stream Mach number, M_0	Wedge half-angle, σ	Pressure recovery		Inlet mass-flow ratio, $\dfrac{m_i}{m_0}$	Estimated wedge mass-flow ratio, $\dfrac{m_w}{m_0}$	Pressure-recovery increase, percent
		Solid wedge	Porous wedge			
1.5	7	0.900	0.932	0.875	0.032	3.6
1.7	9	.872	.927	.925	.050	6.2
1.9	12	.836	.900	.935	.055	7.7
2.0	14	.812	.882	.927	.046	8.6

The comparison was made at equal inlet mass-flow ratios selected near the engine matching condition for the porous wedge. The general level of pressure recovery obtained with the solid wedge at the various Mach numbers was lower than might be expected, considering the favorable Mach number reduction ahead of the inlet that was obtained for 1 and not more than 2 percent total-pressure loss. The wedge surface irregularities caused by the hinge system, particularly at large wedge angles, possibly contributed to its poor performance. The level of pressure recovery was increased by removing 3 to 6 percent of the maximum inlet mass flow by means of area suction through the porous wedge. At Mach numbers greater than 1.5, the pressure recovery was increased 6 to 8.6 percent. The reason for the smaller percentage improvement at a Mach number of 1.5 may be related to lower bleed-air flows and to the slightly greater loss ahead of the inlet. The smaller bleed-air flows may be a result of less pressure difference across the porous material at the lower wedge angles (which provide more optimum shock pressure recovery) and higher duct Mach numbers. Comparison of the wedge bleed mass-flow curves for Mach numbers of 1.5 and 1.9 from figure 6 indicates comparable bleed flows when appreciable normal-shock spillage occurs and the duct-throat Mach numbers are consequently lower.

The increase in minimum drag coefficient due to the porous-wedge exits and bleed flow (although the bleed flows were small for supercritical inlet conditions) was about 0.01 at Mach numbers of 1.5 to 2.0, or roughly 10 percent. Combined effects of drag and pressure recovery will be discussed later in Effective Thrust Comparison.

3979

The use of area suction of the amounts indicated had no significant effect on inlet shock instability other than the shift in minimum exit mass-flow ratio due to bleeding air at the inlet. The greatest stability range for part-throttle engine operation was obtained by operating at the higher or maximum wedge angles.

At a free-stream Mach number of 0.63, back pressure could not be reduced enough to choke the inlet, and hence no supercritical inlet performance was obtained (fig. 7(k)). Since the effect of splitter-plate plan form is believed insignificant for these conditions, the decrease in performance shown for the 12° wedge angle is primarily due to its higher throat Mach numbers because of the reduced throat area. The trend of the data indicates that higher matching pressure recoveries could be attained by decreasing the wedge angle to less than 6°, which would increase the minimum throat area.

The total-pressure distortion $\Delta H/H_{av,2}$ at the compressor-inlet station was decreased in the stable subcritical mass-flow region by reducing the mass-flow ratio or increasing the free-stream Mach number. Area suction or wedge angle had only minor and inconsistent effects on distortion. These trends tend to correlate with the variation of compressor-inlet Mach number or corrected weight flow per unit area (refs. 4 and 5) for subcritical operation.

Effects of Angles of Attack and Yaw

Only minor performance differences were found over the small range of angle of attack investigated (fig. 8). As shown in figure 5, the local Mach number ahead of the inlet was decreased at positive angles and increased to a lesser extent at negative angles of attack. This effect resulted in different capture or supercritical mass-flow ratios. The shifting of the mass-flow - pressure-recovery curves due to different local Mach numbers as well as minor concomitant flow-angularity changes resulted in pressure-recovery variations of less than 1 percent in the stable subcritical mass-flow region. The drag coefficients at positive angles were slightly lower than for zero or negative angles, which is indicative of the effects of the nose droop.

Although the inlet was not sensitive to angle-of-attack effects, under conditions of yaw, asymmetric shock patterns occur on either side of the wedge as well as flow-angularity differences. As shown by the data of figure 9, progressively increasing the yaw angle from 0° to 6° resulted in serious reductions in pressure recovery and appreciably increased drag coefficient and total-pressure distortion. A marked tendency for the inlet to enter regions of unequal duct flow (on either side of the wedge) at reduced mass-flow ratios also occurred as the yaw angle was increased. A method for prediction of the occurrence of this

phenomenon may be found in reference 6. The effect of asymmetrical duct flow is shown by the abnormal variation of distortion and pressure recovery as the mass-flow ratio was reduced.

Diffuser Total-Pressure Distortion

Although the level of maximum total-pressure distortion at the face of the compressor is a valuable guide for judging the effect of distortion on engine performance, the distribution of the flow distortion is likewise important. Circumferential symmetry of flat flow profiles are to be desired. Total-pressure contours selected near engine matching conditions are presented in figure 10 for both $S_cP_0E_0$ and $S_cP_{5.0}E_l$ inlets at Mach numbers of 1.5 to 2.0. Contours for the porous configuration are also shown for a flight Mach number of 0.63 and for a yaw angle of 6^0 at a Mach number of 1.7.

In general, the top portion of the duct had the lowest levels of pressure recovery and the flattest profiles; the highest levels of pressure recovery and the steepest profiles were located near the sides of the duct; the bottom portion of the duct had intermediate pressure-recovery level and profile shape. The cores of higher-energy air found at the duct exit are alined with the sides of the wedge and suggest that mixing action within the diffuser was not sufficient to attain desired distribution of distortion. The effect of wedge-area suction, although not pronounced, was to locally increase radial distortion on the sides and to extend the core of high-energy air somewhat toward the top and bottom. These characteristics are primarily associated with diffuser-area variation, turning or bends, and shape transition rather than inlet conditions such as shock boundary-layer interaction inasmuch as equivalent distributions were obtained at subsonic flight Mach numbers.

Fuselage Boundary-Layer-Removal Scoops

The mass flow captured by the ram-type scoops beneath the splitter plate amounted to between 2 and 3 percent of the maximum inlet mass-flow ratio. This mass-flow ratio was relatively unaffected by wedge angle, angle of attack, normal-shock spillage, or flight Mach number. Angle of yaw decreased the leeward scoop mass flow and increased the windward mass flow; the total mass flow, however, was reduced slightly, for example, from 2.6 to 2.0 percent for 6^0 yaw at a Mach number of 1.7.

Reducing the scoop mass-flow ratio about 10 percent did not influence the performance of the main inlet except near critical flow, where a shock fluctuation existed until the normal shock moved out on the splitter plate. This effect was not found when using the triangular splitter plate.

3979

CE-2 back

Effective Thrust Comparison

Air-flow and thrust characteristics for a conventional two-spool compressor turbojet engine with afterburner were used for computing the ratio of net-thrust-minus-drag to ideal thrust, referred to as the effective thrust ratio hereinafter. Inasmuch as the size of the inlet was designed with allowance made for wedge bleed flow, the solid-wedge inlet was too large for the same engine air flow. Consequently, the size of the solid-wedge inlet was reduced relative to the body size, and the incremental drag (inlet-body minus faired-nose drag coefficient) was reduced according to the size ratio and added to the faired-nose drag coefficient. The size ratio was found to be about 0.9 for near optimum operation over the Mach number range of 1.5 to 2.0. The effect of wedge angle and Mach number for the $S_c P_{5.0} E_l$ inlet on effective thrust ratio, percentage of distortion, and percentage of thrust loss due to drag or pressure recovery at an angle of attack of 2° is shown in figure 11 for an altitude of 35,000 feet. Similar results are shown in figure 12 for optimum (peak effective thrust ratio) wedge-angle schedules for the $S_c P_0 E_0$ and $S_c P_{5.0} E_l$ inlets as well as the performance of a fixed 12° wedge $S_c P_{5.0} E_l$ inlet. The effect of yaw angle is shown in figure 13.

The principal effect of wedge angle on effective thrust ratio for the porous bleed inlet was the percentage of thrust loss due to pressure recovery $(1 - F_n/F_{n,i})$. This varied mainly because of the degree of subcritical or supercritical operation, but also because of shock recovery for the different wedge angles. The drag coefficient as a percentage of ideal thrust $D/F_{n,i}$ was not greatly affected by wedge angle. Likewise, total-pressure distortion was insensitive to wedge angle in spite of differences in the degree of subcritical or supercritical operation. Thus, little opportunity is present for compromising effective thrust by resizing in order to obtain a lower level of distortion. This inability to compromise is primarily due to the dependance of distortion level on duct Mach number or corrected weight flow, as previously discussed, which remains fixed for a given matching condition.

Comparison of optimum variable-angle porous- and solid-wedge inlets (fig. 12) indicates increases in effective thrust for the porous wedge over that for the solid wedge of about 4 percent at a Mach number of 1.5 and almost 10 percent at a Mach number of 2.0. In terms of ideal thrust, bleed increased the effective thrust about 3 percent at a Mach number of 1.5 and about 5 percent at a Mach number of 2.0. Fixing the angle of the porous wedge at 12° resulted in appreciably lower effective thrust ratios at Mach numbers less than 1.7 because of supercritical matching; however, the performance was about equal to that of the variable-angle porous-wedge inlet between Mach numbers of 1.7 and 1.9. Operation at a Mach number of 2.0 was not possible with this fixed wedge angle because of matching in a region of inlet shock instability. For the variable-angle

porous-wedge inlet, the level of distortion decreased from 16 to 6 percent between Mach numbers of 1.5 and 2.0. The variable-angle solid-wedge inlet had a progressively higher level of distortion as the Mach number was decreased from 1.7 to 1.5. This resulted from the use of a fixed scale factor of 0.9, which required matching at supercritical inlet conditions. The level of distortion for the fixed-angle porous-wedge inlet was about comparable with that for a variable-angle porous-wedge inlet. Optimum wedge-angle schedules were slightly different for the porous and solid wedges with the solid wedge tending to favor smaller angles by about 1°.

At matching conditions the ratio of drag to ideal thrust $D/F_{n,i}$ for the solid-wedge inlet was increased over that for the faired nose by about 4 percent of ideal thrust at a Mach number of 2.0 and decreased about 1 percent of ideal thrust at a Mach number of 1.5. Inasmuch as the minimum drag coefficients were nearly equal to the faired-nose values, the region where the inlet body has a larger value of $D/F_{n,i}$ than the faired nose is indicative of subcritical matching and the attendant normal-shock spillage drag. The $S_c P_{5.0} E_l$ inlet matched subcritically by an amount slightly greater than that for the solid-wedge inlet. However, the difference in $D/F_{n,i}$ between the variable-angle porous- and solid-wedge inlets can be interpreted roughly as the increased thrust loss due to the porous-wedge air flow and the drag reduction due to the smaller size of the solid-wedge inlet. This difference varied from about $1\frac{1}{2}$ to $2\frac{1}{2}$ percent of ideal thrust between Mach numbers of 1.5 and 2.0 for wedge air flows of 3 to 6 percent of the maximum inlet capture mass flow. The increased thrust due to pressure-recovery gains through the use of area suction varied between 5 and 8 percent of ideal thrust. The net result of increased drag and pressure recovery due to area suction has been discussed previously.

Effective thrust ratio was progressively decreased as yaw angle was increased to 6° by about 10 percent of ideal thrust at a Mach number of 1.6 and by about 15 percent at a Mach number of 1.9 for wedge angles that did not enter supercritical flow at the matching condition (fig. 13). The loss in effective thrust was as much as 20 percent for wedge angles that matched supercritically. In general, the flow distortion at the matching condition was not greatly increased by yaw since matching occurred at mass-flow ratios higher than the region of serious asymmetrical shock structure. A notable exception, however, is shown by the 10° wedge angle at a Mach number of 1.8, which apparently encountered asymmetrical flow at mass-flow ratios only slightly less than critical (as contrasted with other wedge angles) as yaw angle was increased.

As would be expected from the data shown in figure 8, angles of attack between $\pm 4^{\circ}$ resulted in only small reductions in effective thrust and the results are not presented.

SUMMARY OF RESULTS

An underslung inlet having a variable-angle vertical-wedge compression surface was tested at Mach numbers of 0.63 and 1.5 to 2.0, angles of attack between $\pm 4^{\circ}$, and angles of yaw from 0° to 6°. Data were taken for nonporous as well as two porous wedges. The porous-wedge sections (3.5- or 5-percent open area) occupied about 20 percent of the length of the wedge in the region of the inlet throat. An analysis of a wedge position control device is presented in the appendix. The following results were obtained:

1. The subcritical level of pressure recovery between Mach numbers of 1.5 and 2.0 for the solid-wedge inlet was low by comparison with other inlets considering that the local Mach number ahead of the inlet was reduced by about 0.10 for about a 1-percent loss in total pressure. However, by removing 3 to 6 percent of the maximum inlet mass flow by means of area suction through the porous wedge, pressure recovery was increased about 3.6 percent at a Mach number of 1.5 and about 8.6 percent at a Mach number of 2.0.

2. In general, increasing the wedge bleed flow by increasing the porosity resulted in progressive improvement in pressure recovery at Mach numbers greater than 1.5. For the solid wedge, bleed-flow rates of about 1 percent applied at the wedge hinge and clearance spaces increased the pressure recovery 3 and 1 percent at Mach numbers of 1.9 and 1.5, respectively.

3. At engine matching conditions increases in pressure recovery due to bleed from the porous wedge increased effective thrust between 5 and 8 percent of ideal engine thrust. Drag associated with ingesting and discharging 3 to 6 percent of the wedge bleed air and with the larger-size inlet needed for internal bleed was approximately $1\frac{1}{2}$ to $2\frac{1}{2}$ percent of ideal thrust. The combined effect was an effective-thrust-ratio increase of about 3 and 5 percent of ideal thrust at Mach numbers of 1.5 and 2.0, respectively.

4. Altering the form of the splitter plate that separated the compression surface from the fuselage boundary layer increased the pressure recovery about 2 percent and the captured mass flow about 1 percent at Mach numbers greater than 1.5.

5. Angles of attack between $\pm 4^{\circ}$ had only small effects on inlet performance because of the favorable inlet location on the fuselage. However, angles of yaw up to 6° seriously decreased pressure recovery and increased drag. For angles of yaw of 6° the effective thrust ratio was decreased between 10 and 15 percent of ideal thrust.

6. At engine matching conditions for a schedule of optimum wedge angles, the total-pressure distortion at the compressor inlet was decreased from a value of 16 percent at a Mach number of 1.5 to about 6 percent at a Mach number of 2.0. Area suction or wedge angle had only minor effects on distortion.

7. The distribution of distortion at the compressor-inlet station featured large regions of low-energy air at the top and to a lesser extent at the bottom of the duct with cores of high-energy air alined with the sides of the wedge. This was characteristic subsonically as well as supersonically and hence is associated with diffuser duct geometry.

8. Wedge static-pressure taps provided an input signal of such a nature that for the zero-yaw condition a wedge position control device could maintain effective thrust within 1 percent of the optimum value.

Lewis Flight Propulsion Laboratory
    National Advisory Committee for Aeronautics
   Cleveland, Ohio, February 29, 1956

3979

APPENDIX - CONSIDERATIONS FOR NORMAL-SHOCK CONTROL OF

VARIABLE-WEDGE INLETS

By Fred Wilcox and Norman Musialowski

Inlet normal-shock sensing has been used as a control parameter for positioning the translating spike of an axisymmetric inlet (ref. 7) as the engine air-flow requirements changed. This same principle may also be applied to a side inlet equipped with a variable-angle wedge, whereby the wedge angle is varied so as to maintain the normal shock at the cowl lip over a range of operating conditions. Such an application is schematically illustrated in the following sketches:

$p_s \approx p_r$ $p_s > p_r$
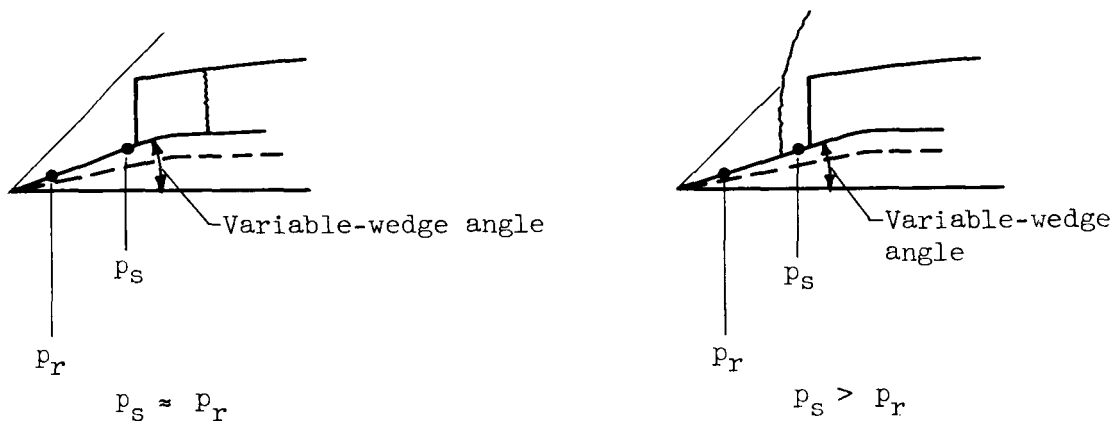
(a) Supercritical inlet operation.   (b) Subcritical inlet operation.

A static pressure p_s (normal-shock-position sensing pressure) is measured on the wedge surface at a point where it is desired to locate the inlet normal shock. Another static pressure p_r is measured forward on the wedge surface and is used as a reference. In sketch (a) the inlet operation is supercritical, and because of the downstream location of the normal shock, the sensing pressure is approximately equal to the reference pressure. In order to obtain critical inlet operation, the wedge angle would have to be decreased, causing less air to be spilled behind the inlet oblique shock. The action to be taken by the control when p_s is approximately equal to p_r would thus be to decrease the wedge angle.

Subcritical inlet operation is illustrated in sketch (b). In this case p_s is considerably greater than p_r, because the normal shock is located ahead of the sensing orifice to spill excess air. By increasing the wedge angle, the amount of air spilled behind the oblique shock will increase and the inlet operating point will move toward critical. The control action should, therefore, be to increase the wedge angle when p_s is greater than p_r. Thus, for a certain value of corrected weight flow

3979

CE-3

per unit area or Mach number set by the engine operating condition, the action of the control is to adjust oblique-shock spillage by varying the wedge angle until the normal shock is positioned at the sensing orifice.

The specific inlet discussed in this report was designed with two oblique shocks rather than the single one of this example. In addition, the two side inlets were placed back to back, and the same mechanism was utilized to actuate both wedges simultaneously. Data obtained with wall static orifices on the ramp behind the second oblique shock were investigated to determine whether the preceding principles could be applied to the control of this inlet. The normal-shock-position sensing pressure was obtained by averaging the readings from orifices on opposite sides of the inlet (fig. 3). The reference pressure was obtained in a similar manner.

The control signal data obtained are presented in parameter form in figure 14 by dividing the difference between the averaged sensing and averaged reference pressures by the free-stream static pressure. This is done to make the data independent of altitude (ref. 8). Data are presented for several second wedge angles over a range of inlet air flows at free-stream Mach numbers of 1.5, 1.8, and 2.0. Also shown on the figure are the engine matching line and a suggested control setting. The wedge angle which would be set by the control can be obtained by interpolating at the intersection of the control setting and the engine matching line. For example, at a flight Mach number of 1.5 and a control setting of 0.20, the control would set a wedge angle of about 8.0°.

It appears possible to obtain good inlet performance for a wide range of control settings inasmuch as optimum thrust-minus-drag is not appreciably decreased by slight variations of wedge angle (fig. 11). Because of this wide permissible range of control setting indicated on figure 14, it should be possible to operate a control of this type over a range of altitude without requiring scheduling of the control setting with altitude.

The excellence of the control signal obtained over the range of Mach number and angle of attack is attributed mainly to the boundary-layer-removal system built into the inlet ahead of the normal-shock-position sensing orifice. The two-oblique-shock configuration used had the effect of maintaining the strength of the normal shock more nearly constant than would be obtained with a single wedge over a range of free-stream Mach numbers. This accounted in part for the rather uniform control signal value obtained as the free-stream Mach number was raised.

Angles of attack from 0° to $\pm 4^{\circ}$ (the range investigated) had negligible effect on the control signal. Examination of the data obtained at angles of yaw to 6° indicated that no usable signal was obtained from the windward side because the normal shock was swallowed on this side.

A signal was obtained from the leeward side which would control the inlet close to the optimum operating point. Averaging the signals from both sides, however, results in a poor control signal.

The inlet performance estimated from the control signal data of figure 14 and the data of figure 11 is shown in figure 15 for a range of control settings. This figure shows that within the accuracy of the tests a control based on the principle described and set within static-pressure-parameter limits of 0 to 0.70 should set the wedge to give inlet performance within 1 percent of optimum over the Mach number range covered. A static-pressure-parameter value of 0.2 indicates performance even closer to optimum.

3979

REFERENCES

1. Esenwein, Fred T.: Performance Characteristics at Mach Numbers to 2.00 of Various Types of Side Inlets Mounted on Fuselage of Proposed Supersonic Airplane. III - Normal-Wedge Inlet with Semicircular Cowl. NACA RM E52H20, 1952.

2. Weinstein, M. I.: Performance of Supersonic Scoop Inlets. NACA RM E52A22, 1952.

3. Hasel, Lowell E.: Investigation at Mach Numbers of 1.41, 1.61, and 1.82 of Two Variable-Geometry Inlets Having Two-Dimensional Compression Surfaces. NACA RM L54K04, 1956.

4. Piercy, Thomas G.: Factors Affecting Flow Distortions Produced by Supersonic Inlets. NACA RM E55L19, 1956.

5. Sterbentz, William: Factors Controlling Air-Inlet Flow Distortions. NACA RM E56A30, 1956.

6. Beke, Andrew: Criteria for Initial Flow Reversal in Symmetrical Twin-Intake Air-Induction Systems Operating at Supersonic Speeds. NACA RM E55L02a, 1956.

7. Leissler, L. Abbott, and Nettles, J. Cary: Investigation to Mach Number 2.0 of Shock-Positioning Control Systems for a Variable-Geometry Inlet in Combination with a J34 Turbojet Engine. NACA RM E52I27, 1954.

8. Wilcox, Fred A., and Perchonok, Eugene: Aerodynamic Control of Supersonic Inlets for Optimum Performance. NACA RM E55L14, 1956.

DECLASSIFIED

CE-3 back

Section A-A

Section B-B

Porous-wedge air control valve

Section C-C

Section D-D

Section E-E

Section F-F

Boundary-layer air ducts

Section G-G

Porous-wedge metering nozzle

Porous-wedge air exits

Boundary-layer air exit

Section H-H

Compressor-inlet station

Labyrinth seal

H

Rear lift link

G

G

Strain-gage balance

Boundary-layer air ducts

Side force bearings

Porous-wedge inlet

Outline of faired nose

H

A

B

C

D

A

B

C

D

E

F

E

F

Mass-flow control plug

Metering nozzle

4 Flow-straightening screens

To tunnel support strut

CD-4992

Model station

0   10   20   30   40   50   60   70   80   90   100   110   120   130   140

Model station

130   140   150   160   170   180   190   200   210   220   230   240   250   260

Figure 1. - Schematic diagram of model.

NACA RM E56B15

3979

(a) Three-quarter front view; cutback splitter plate.

(b) Three-quarter front view; triangular splitter plate.

(c) Front view; minimum wedge angle, 6°; cutback splitter plate.

C-41309

Figure 2. - Photographs of inlet.

DECLASSIFIED

Figure 3. - Details of wedge hinge system, porosity distribution, boundary-layer scoop and diverter, and splitter-plate plan forms.
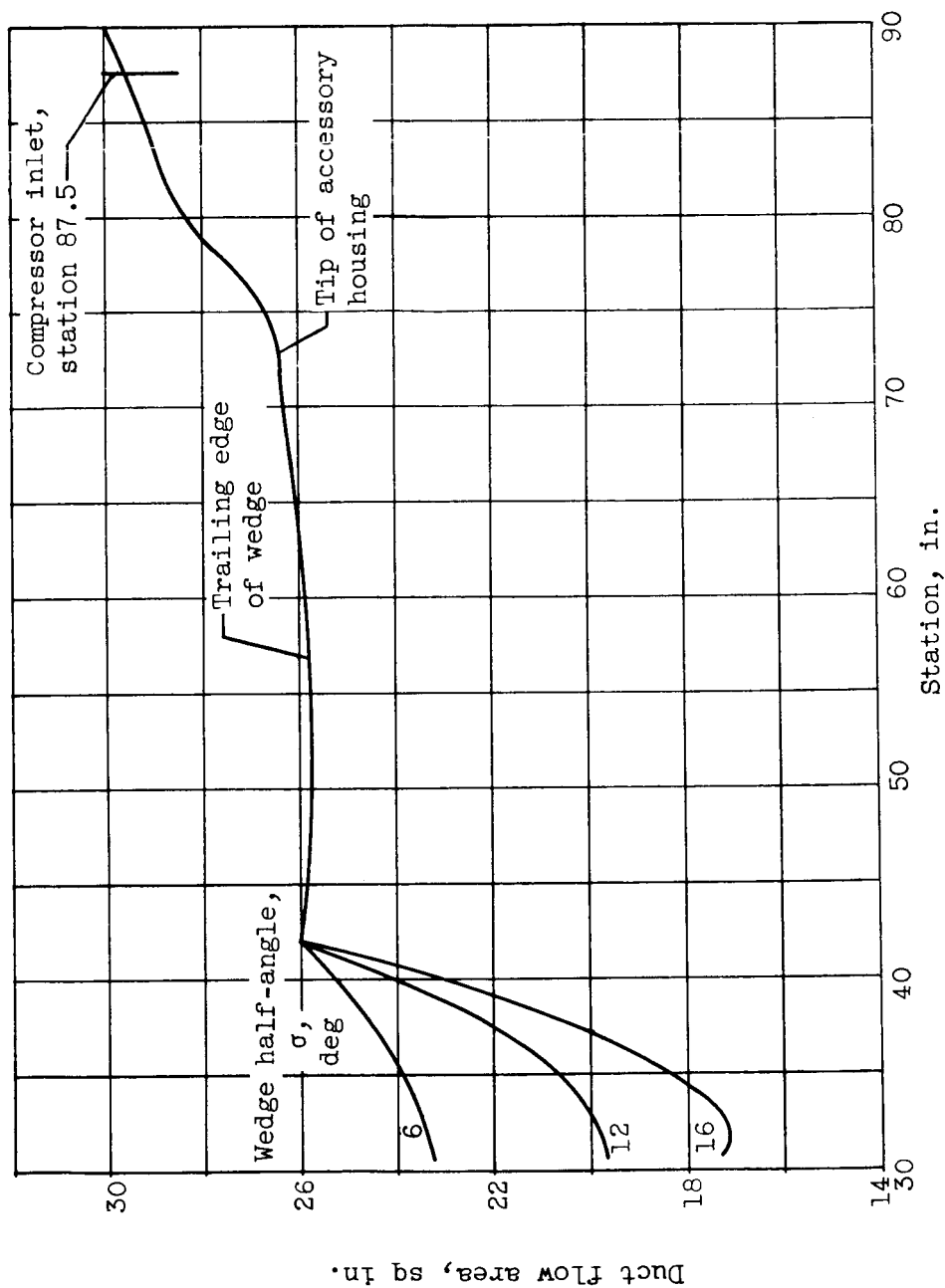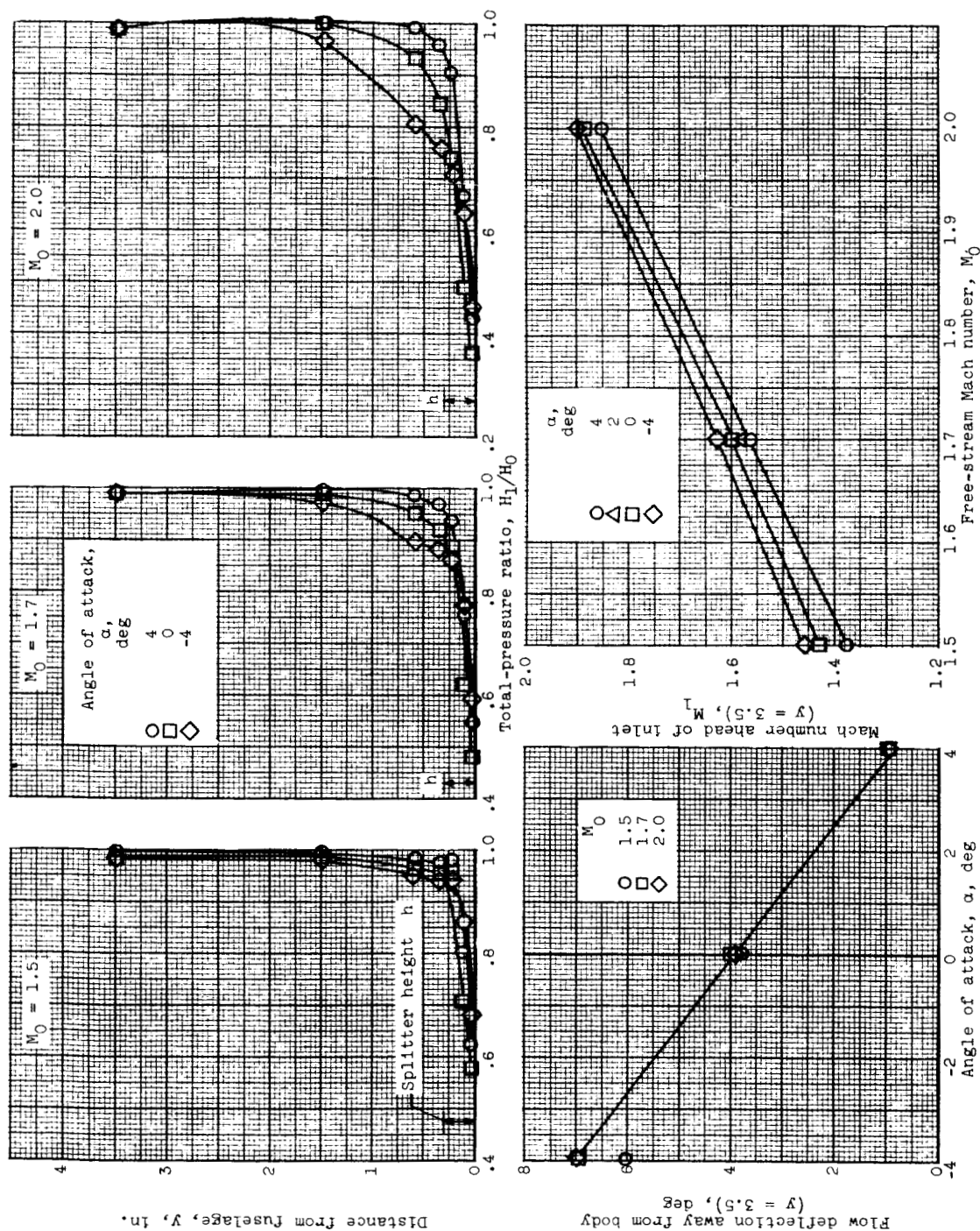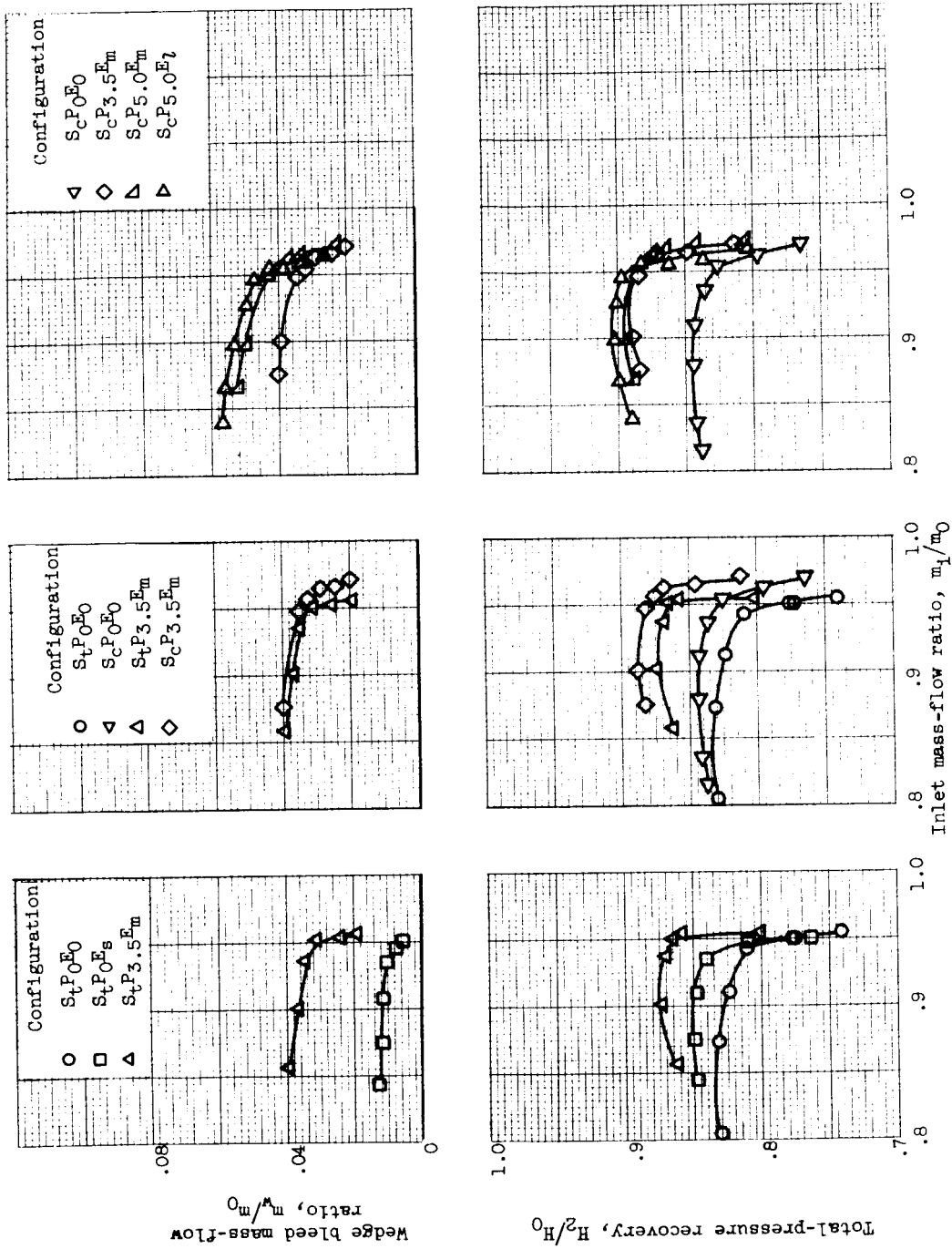
Figure 4. - Subsonic-diffuser-area variation.

3979

Figure 5. - Inlet flow-field survey. Zero angle of yaw.

(a) Flight Mach number, 1.9; wedge half-angle, 12°.

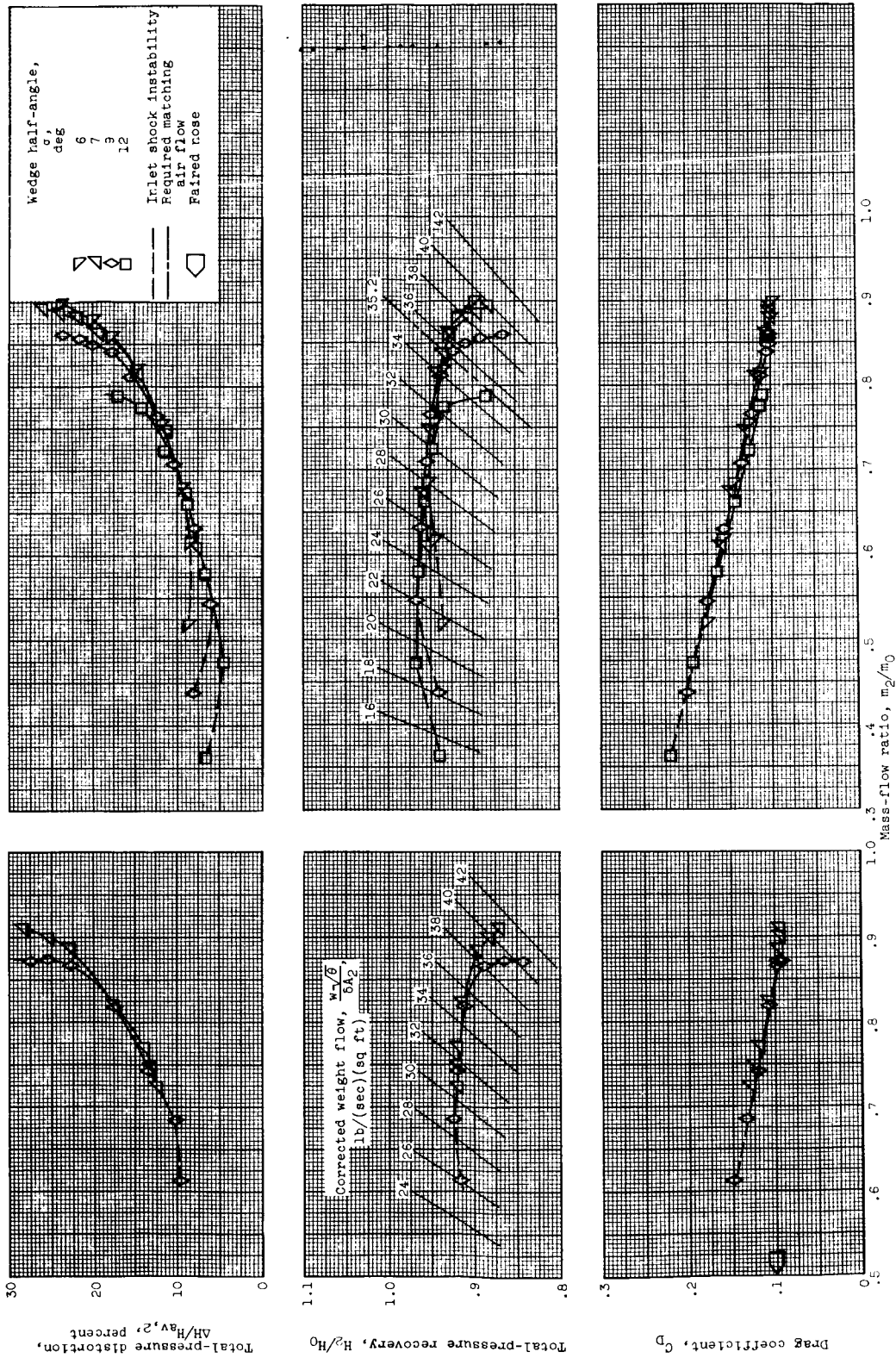Figure 6. - Comparison of inlet configurations. Angle of attack, 2°.

3979

CE-4
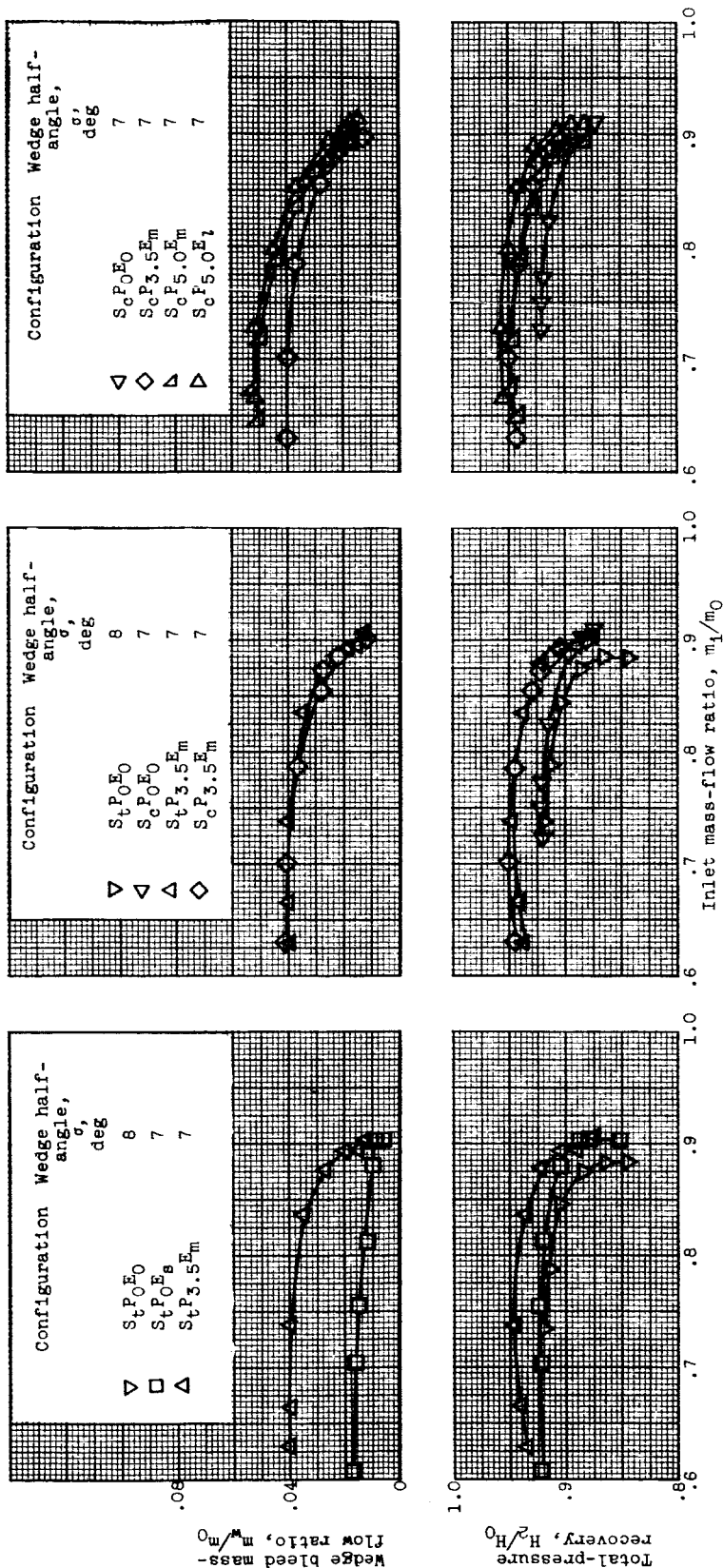
Figure 6. - Concluded. Comparison of inlet configurations. Angle of attack, 2°.
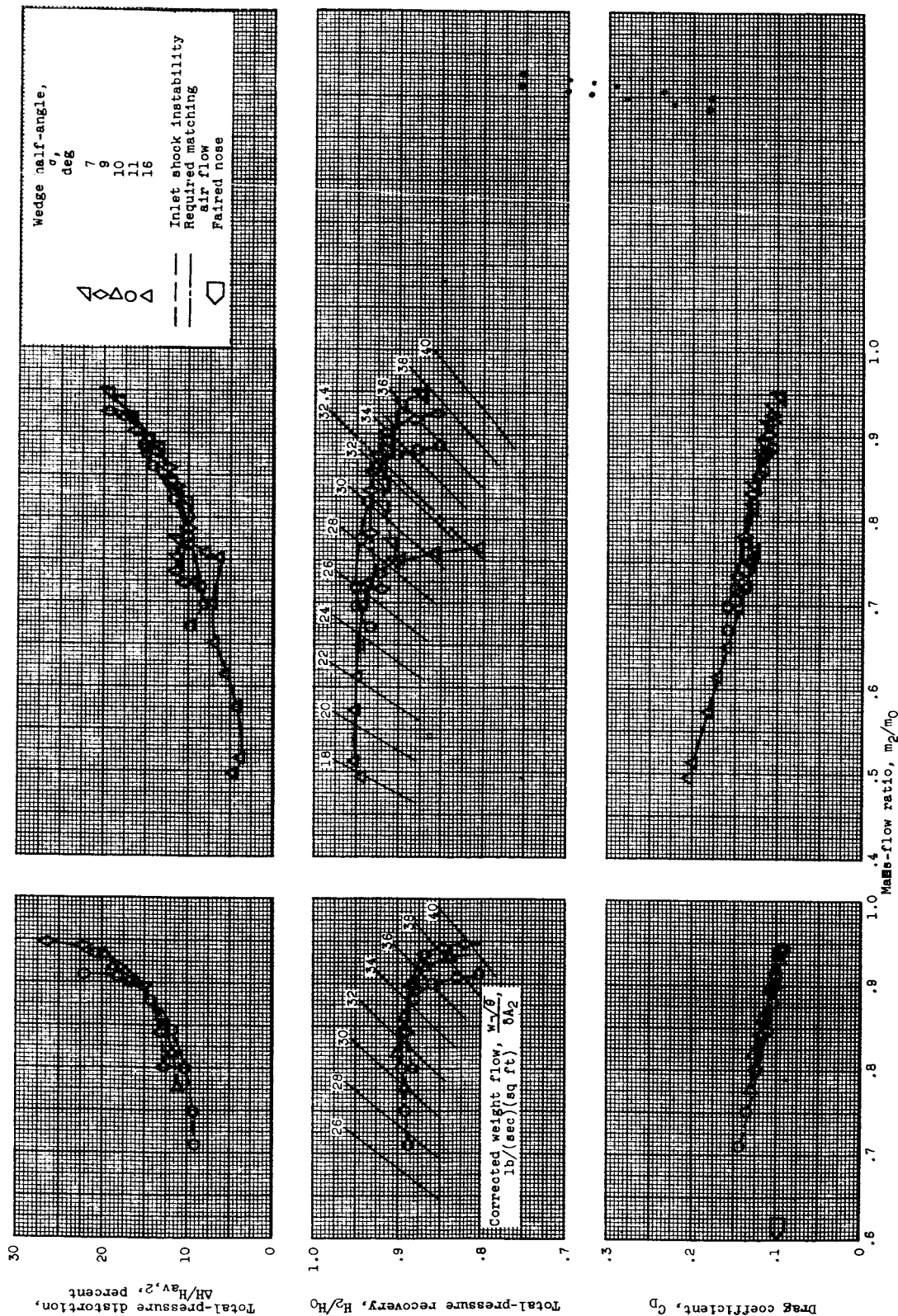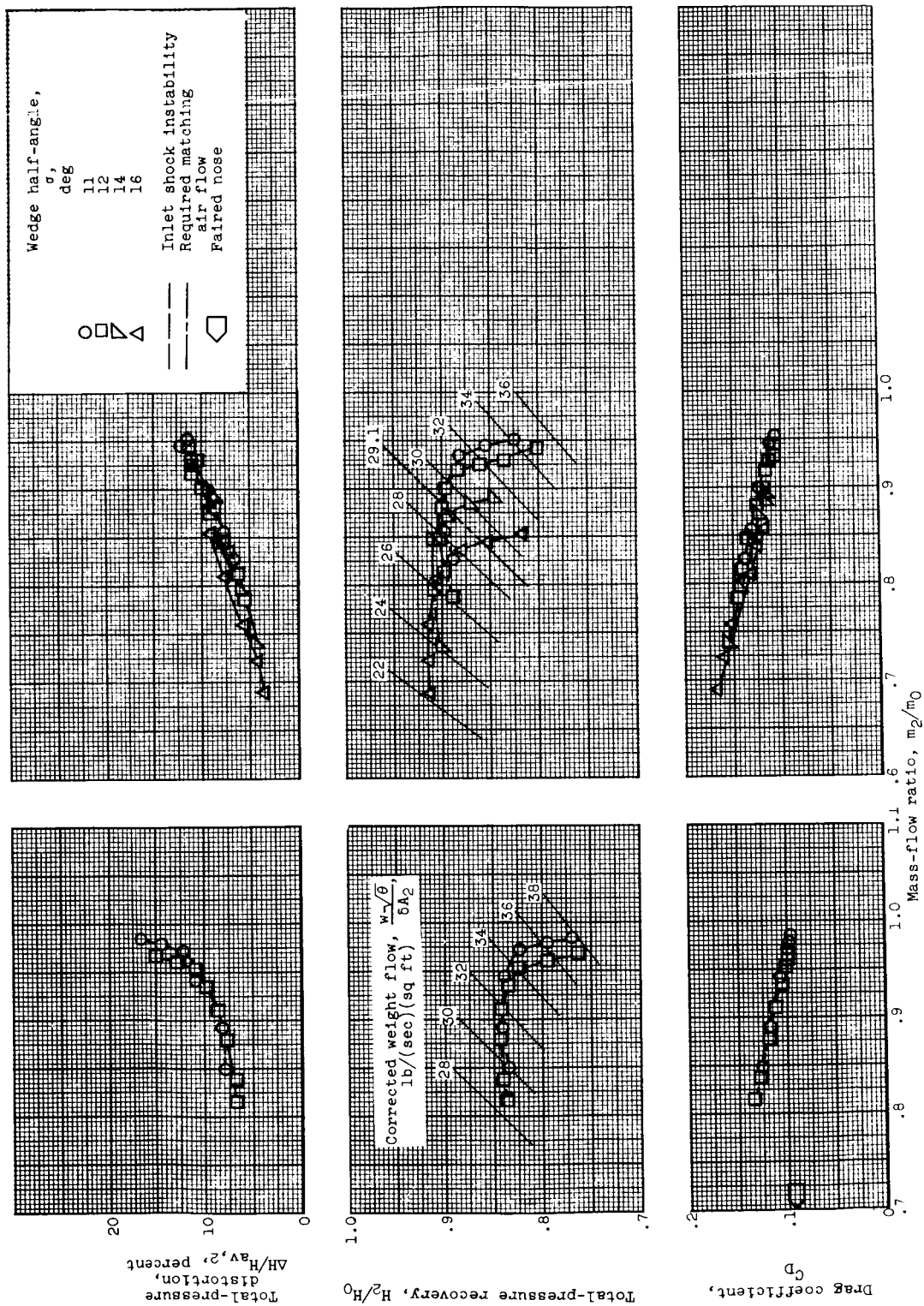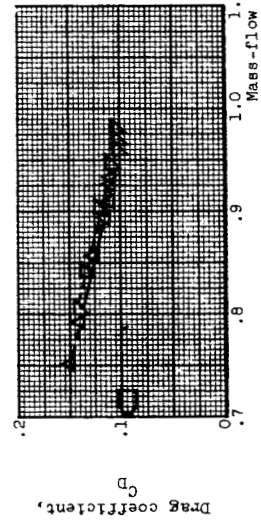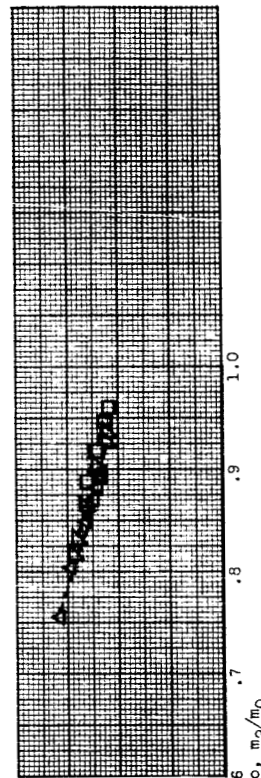
(b) Flight Mach number, 1.5.

Inlet mass-flow ratio, m_1/m_0

(a) Free-stream Mach number, 1.5; solid wedge $S_cP_0E_0$.

(b) Free-stream Mach number, 1.5; porous wedge $S_cP_5.0E_1$.

Figure 7. - Inlet performance with solid and porous wedges. Angle of attack, $2°$.
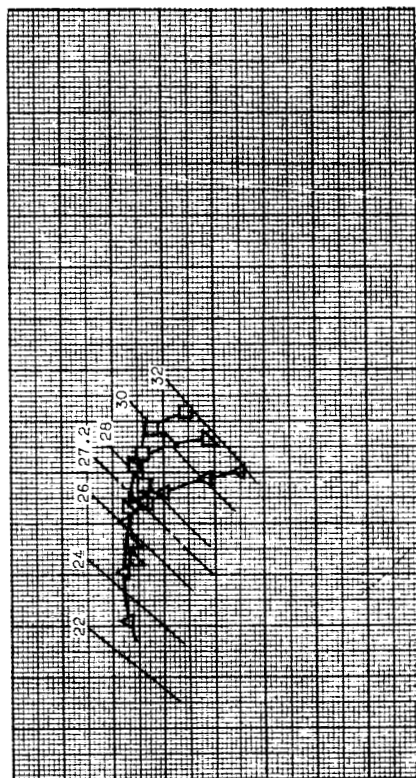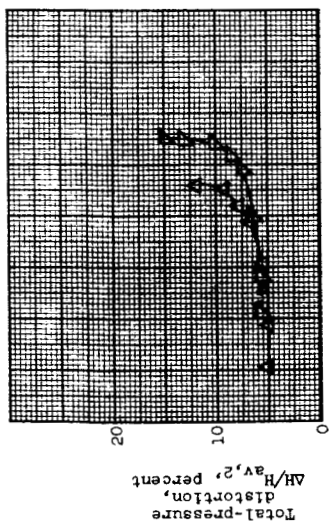
Figure 7. - Continued. Inlet performance with solid and porous wedges. Angle of attack, 2°.

(c) Free-stream Mach number, 1.7; solid wedge $S_c P_0 E_0$.

(d) Free-stream Mach number, 1.7; porous wedge $S_c P_5, 0 E_1$.

3979

Wedge half-angle,
σ,
deg
11
12
14
16

Inlet shock instability
Required matching air flow
Faired nose

Total-pressure distortion, ΔH/H_{av,2}, percent

Corrected weight flow, $\frac{w\sqrt{\theta}}{\delta A_2}$, lb/(sec)(sq ft)

Total-pressure recovery, H_2/H_0

Drag coefficient, C_D

Mass-flow ratio, m_2/m_0

(e) Free-stream Mach number, 1.9; solid wedge $S_c P_0 E_0$.

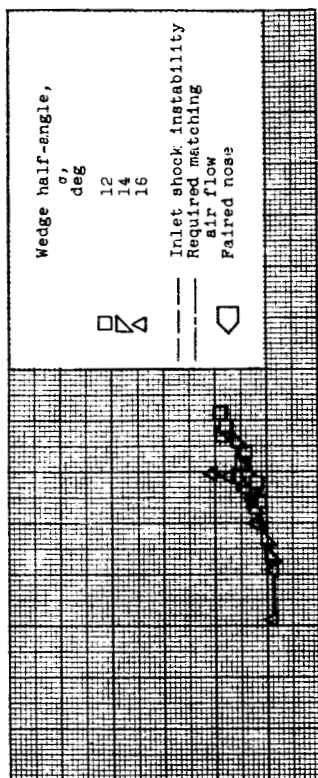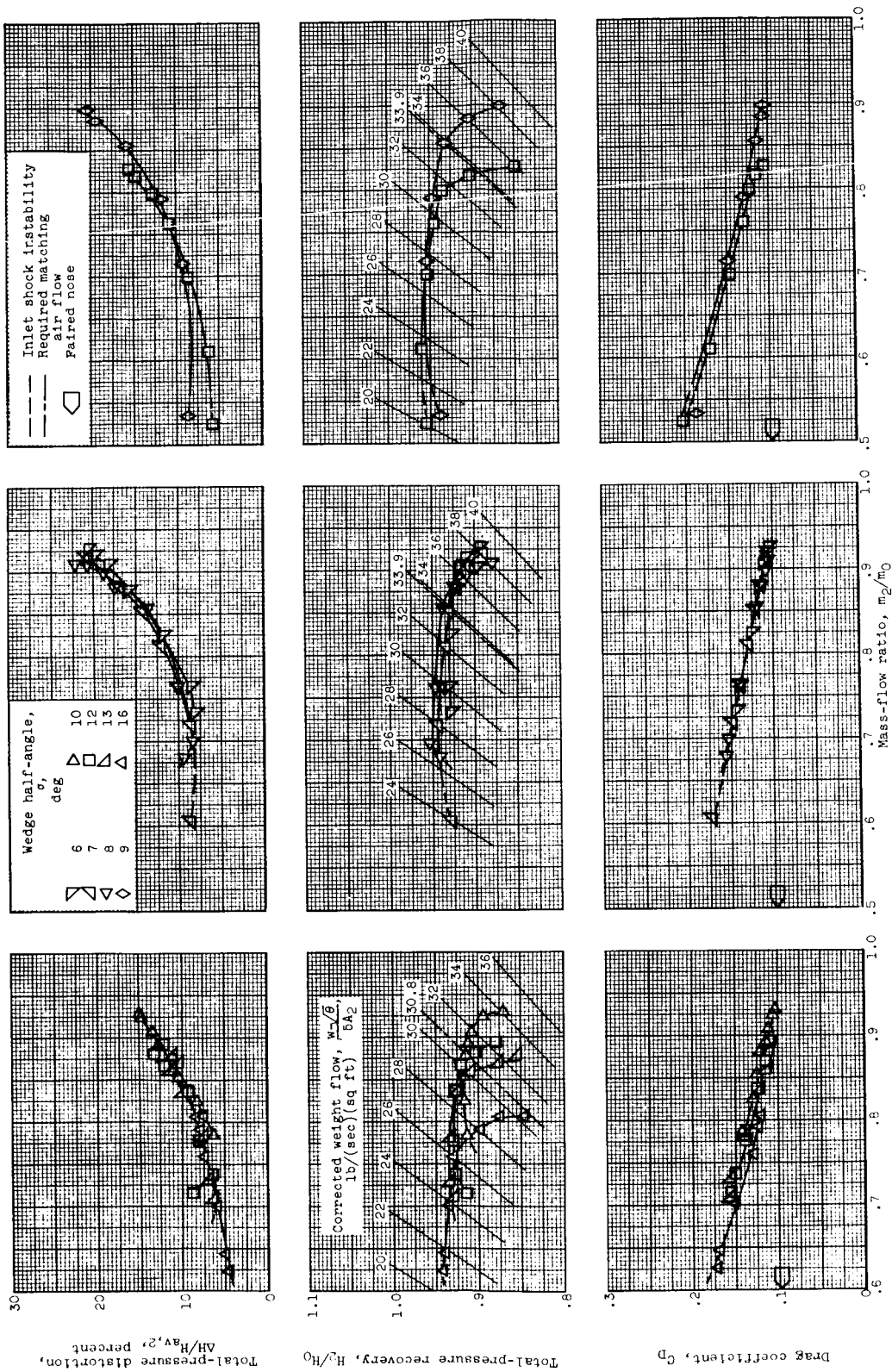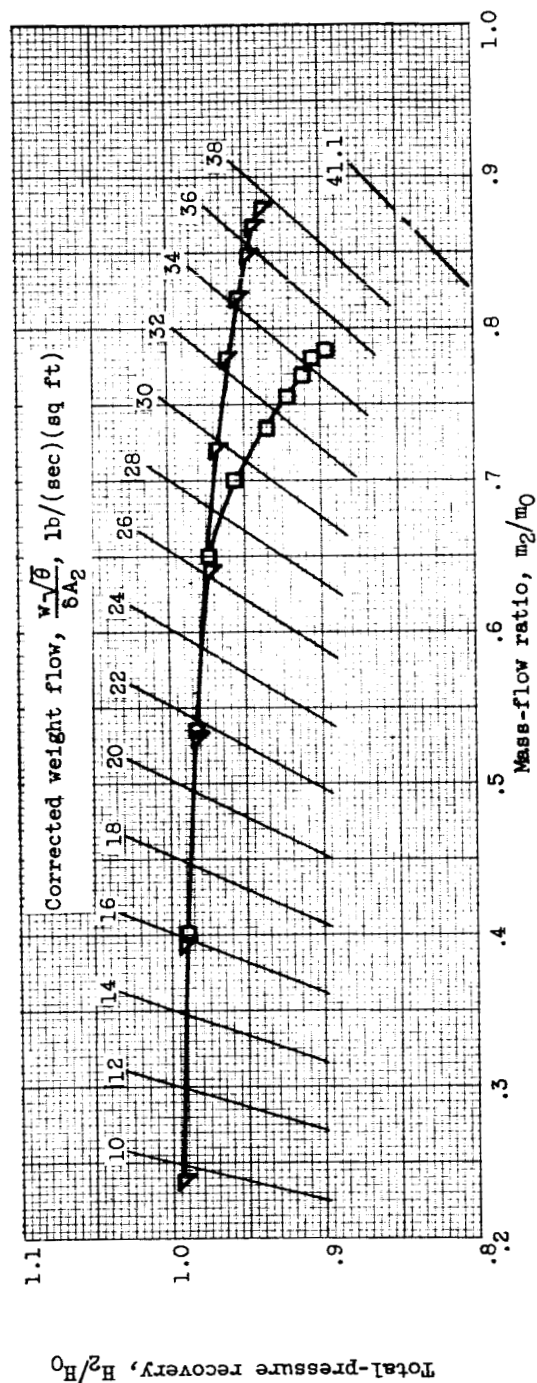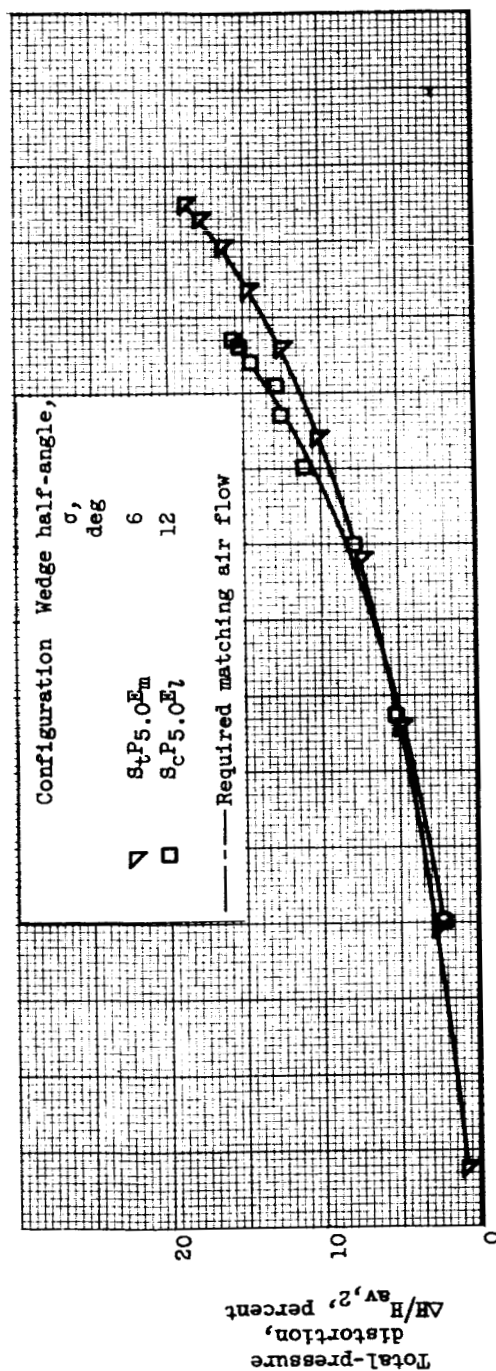(f) Free-stream Mach number, 1.9; porous wedge $S_c P_5 O E_1$. Angle of attack, $2°$.

Figure 7. - Continued. Inlet performance with solid and porous wedges. Angle of attack, $2°$.

3979

(g) Free-stream Mach number, 2.0; solid wedge $S_C P_0 E_0$.

(h) Free-stream Mach number, 2.0; porous wedge $S_C P_5, _0 E_1$.

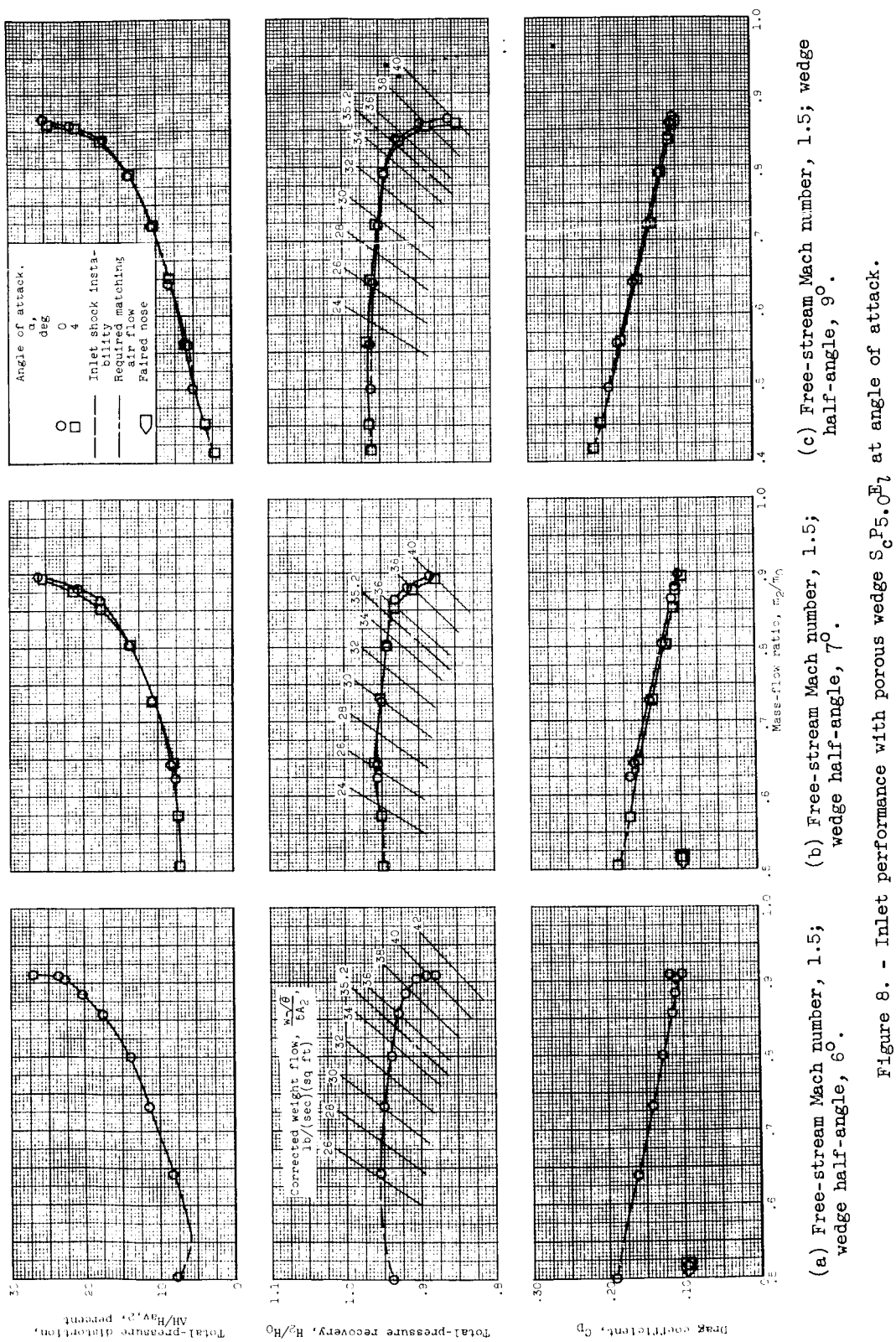Figure 7. - Continued. Inlet performance with solid and porous wedges. Angle of attack, 2°.

(i) Free-stream Mach number, 1.8; porous wedge S_cP_5,OE_i.

(j) Free-stream Mach number, 1.6; porous wedge S_cP_5,OE_i.

Figure 7. - Continued. Inlet performance with solid and porous wedges. Angle of attack, 2°.

3979
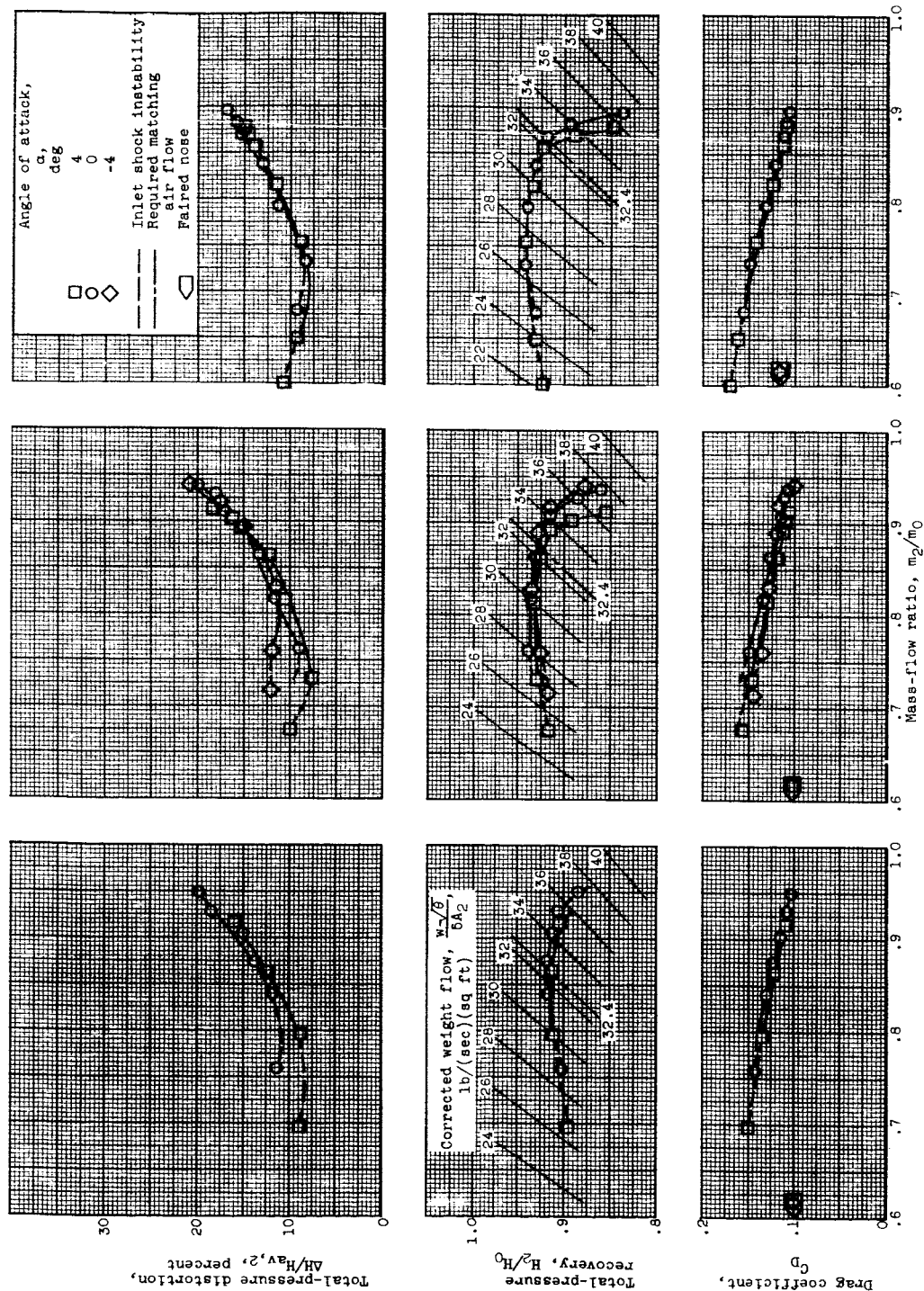

(k) Free-stream Mach number, 0.63.

Figure 7. - Concluded. Inlet performance with solid and porous wedges. Angle of attack, 2°.

(a) Free-stream Mach number, 1.5; wedge half-angle, 6°.

(b) Free-stream Mach number, 1.5; wedge half-angle, 7°.

(c) Free-stream Mach number, 1.5; wedge half-angle, 9°.

Figure 8. - Inlet performance with porous wedge $S_c P_{5.0} E_7$ at angle of attack.

3979

CE-5

(d) Free-stream Mach number, 1.7; wedge half-angle, 7°.

(e) Free-stream Mach number, 1.7; wedge half-angle, 9°.

(f) Free-stream Mach number, 1.7; wedge half-angle, 11°.

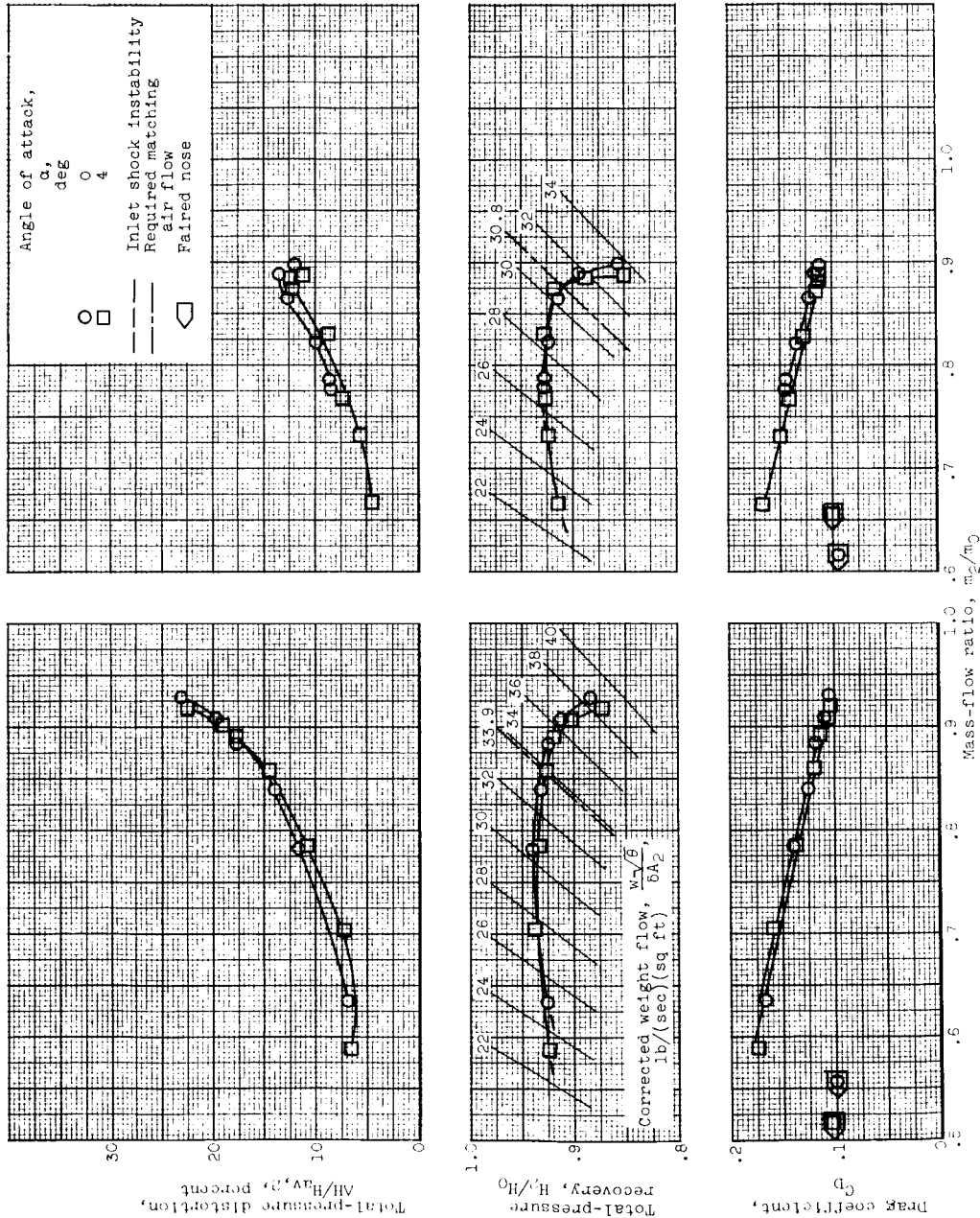Figure 8. - Continued. Inlet performance with porous wedge $S_cP_5{,}_0E_l$ at angle of attack.

3979

3979

CE-5 back

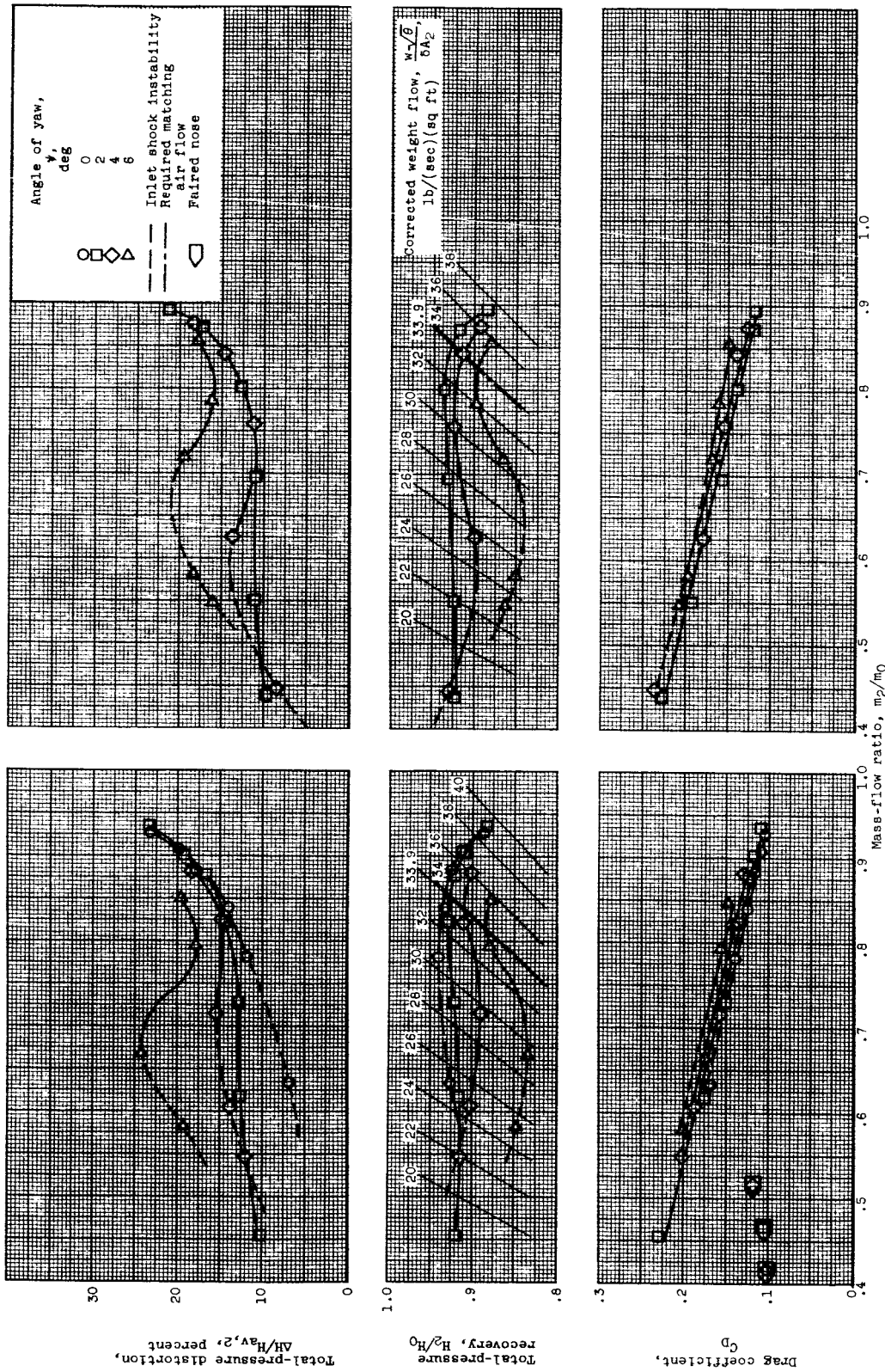(a) Free-stream Mach number, 1.6; wedge half-angle, 7°.

(b) Free-stream Mach number, 1.6; wedge half-angle, 9°.

Figure 9. - Inlet performance with porous wedge $S_cP_{5.0}E_1$ at angles of yaw. Zero angle of attack.
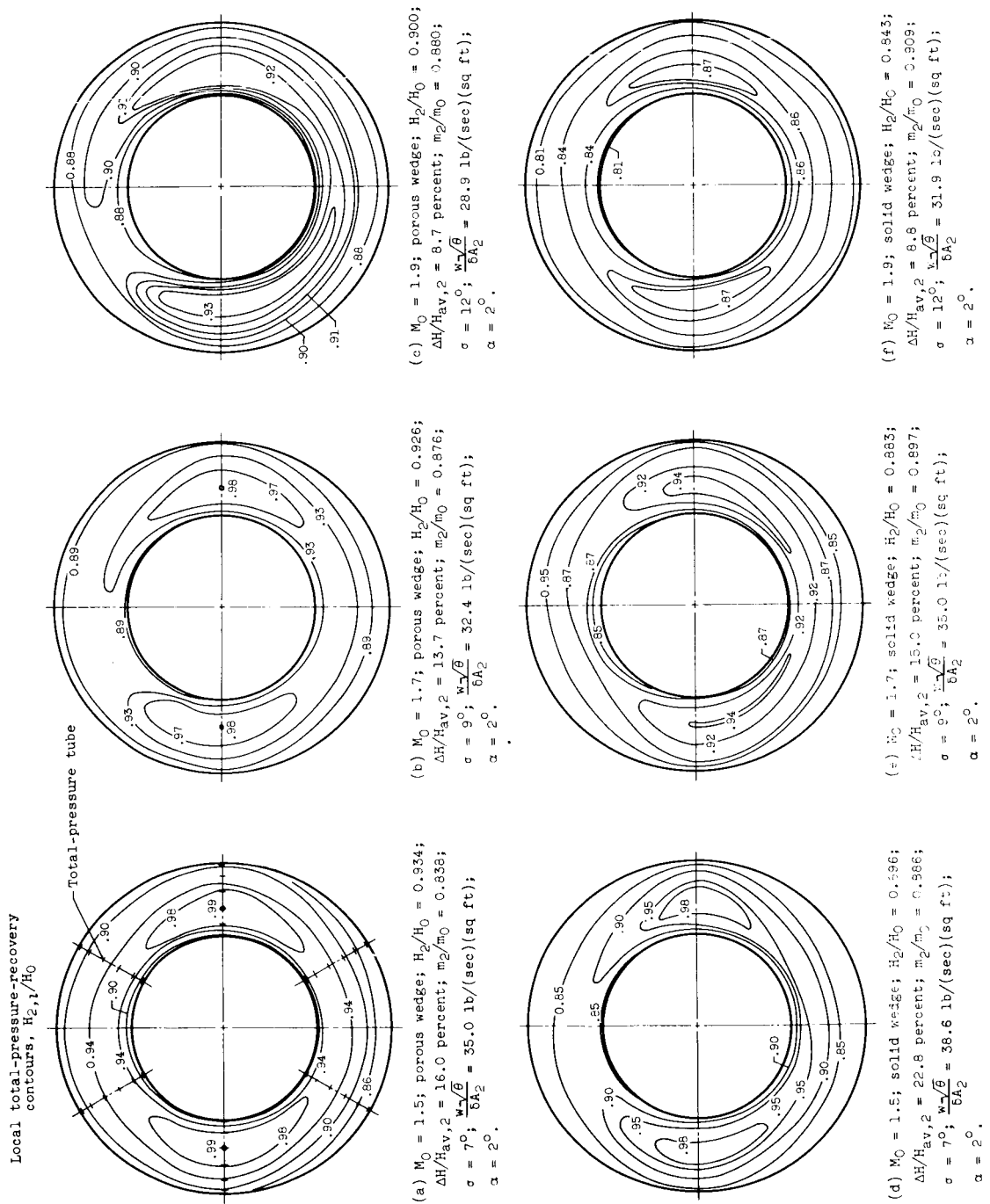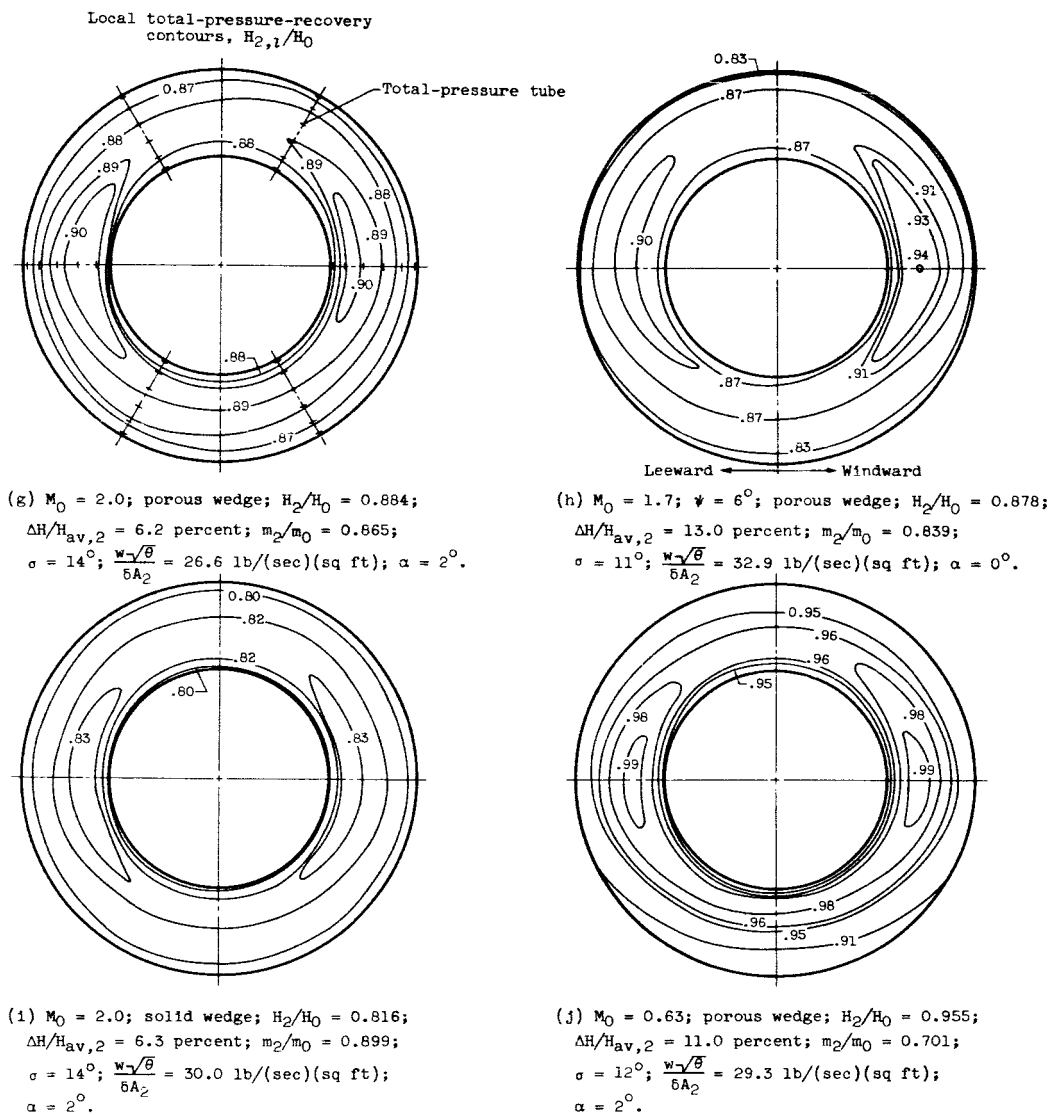
Local total-pressure-recovery
contours, $H_{2,1}/H_0$

Total-pressure tube

(a) $M_0 = 1.5$; porous wedge; $H_2/H_0 = 0.934$;
$\Delta H/H_{av,2} = 16.0$ percent; $m_2/m_0 = 0.838$;
$\sigma = 7°$; $\frac{w\sqrt{\theta}}{\delta A_2} = 35.0$ lb/(sec)(sq ft);
$\alpha = 2°$.

(b) $M_0 = 1.7$; porous wedge; $H_2/H_0 = 0.926$;
$\Delta H/H_{av,2} = 13.7$ percent; $m_2/m_0 = 0.876$;
$\sigma = 9°$; $\frac{w\sqrt{\theta}}{\delta A_2} = 32.4$ lb/(sec)(sq ft);
$\alpha = 2°$.

(c) $M_0 = 1.9$; porous wedge; $H_2/H_0 = 0.900$;
$\Delta H/H_{av,2} = 8.7$ percent; $m_2/m_0 = 0.880$;
$\sigma = 12°$; $\frac{w\sqrt{\theta}}{\delta A_2} = 28.9$ lb/(sec)(sq ft);
$\alpha = 2°$.

(d) $M_0 = 1.5$; solid wedge; $H_2/H_0 = 0.896$;
$\Delta H/H_{av,2} = 22.8$ percent; $m_2/m_0 = 0.866$;
$\sigma = 7°$; $\frac{w\sqrt{\theta}}{\delta A_2} = 38.6$ lb/(sec)(sq ft);
$\alpha = 2°$.

(e) $M_0 = 1.7$; solid wedge; $H_2/H_0 = 0.883$;
$\Delta H/H_{av,2} = 15.0$ percent; $m_2/m_0 = 0.897$;
$\sigma = 9°$; $\frac{w\sqrt{\theta}}{\delta A_2} = 35.0$ lb/(sec)(sq ft);
$\alpha = 2°$.

(f) $M_0 = 1.9$; solid wedge; $H_2/H_0 = 0.843$;
$\Delta H/H_{av,2} = 8.8$ percent; $m_2/m_0 = 0.909$;
$\sigma = 12°$; $\frac{w\sqrt{\theta}}{\delta A_2} = 31.9$ lb/(sec)(sq ft);
$\alpha = 2°$.

Figure 10. - Compressor-inlet total-pressure contours for solid wedge $S_cP_5_0E_l$ and porous wedge $S_cP_5_0E_l$.

DECLASSIFIED

3979

Local total-pressure-recovery
contours, $H_{2,l}/H_0$

Total-pressure tube

Leeward ← → Windward

(g) $M_0 = 2.0$; porous wedge; $H_2/H_0 = 0.884$;
$\Delta H/H_{av,2} = 6.2$ percent; $m_2/m_0 = 0.865$;
$\sigma = 14°$; $\frac{w\sqrt{\theta}}{\delta A_2} = 26.6$ lb/(sec)(sq ft); $\alpha = 2°$.

(h) $M_0 = 1.7$; $\psi = 6°$; porous wedge; $H_2/H_0 = 0.878$;
$\Delta H/H_{av,2} = 13.0$ percent; $m_2/m_0 = 0.839$;
$\sigma = 11°$; $\frac{w\sqrt{\theta}}{\delta A_2} = 32.9$ lb/(sec)(sq ft); $\alpha = 0°$.

(i) $M_0 = 2.0$; solid wedge; $H_2/H_0 = 0.816$;
$\Delta H/H_{av,2} = 6.3$ percent; $m_2/m_0 = 0.899$;
$\sigma = 14°$; $\frac{w\sqrt{\theta}}{\delta A_2} = 30.0$ lb/(sec)(sq ft);
$\alpha = 2°$.

(j) $M_0 = 0.63$; porous wedge; $H_2/H_0 = 0.955$;
$\Delta H/H_{av,2} = 11.0$ percent; $m_2/m_0 = 0.701$;
$\sigma = 12°$; $\frac{w\sqrt{\theta}}{\delta A_2} = 29.3$ lb/(sec)(sq ft);
$\alpha = 2°$.

Figure 10. - Concluded.　Compressor-inlet total-pressure contours for solid wedge $S_c P_0 E_0$ and porous wedge $S_c P_{5.0} E_l$.
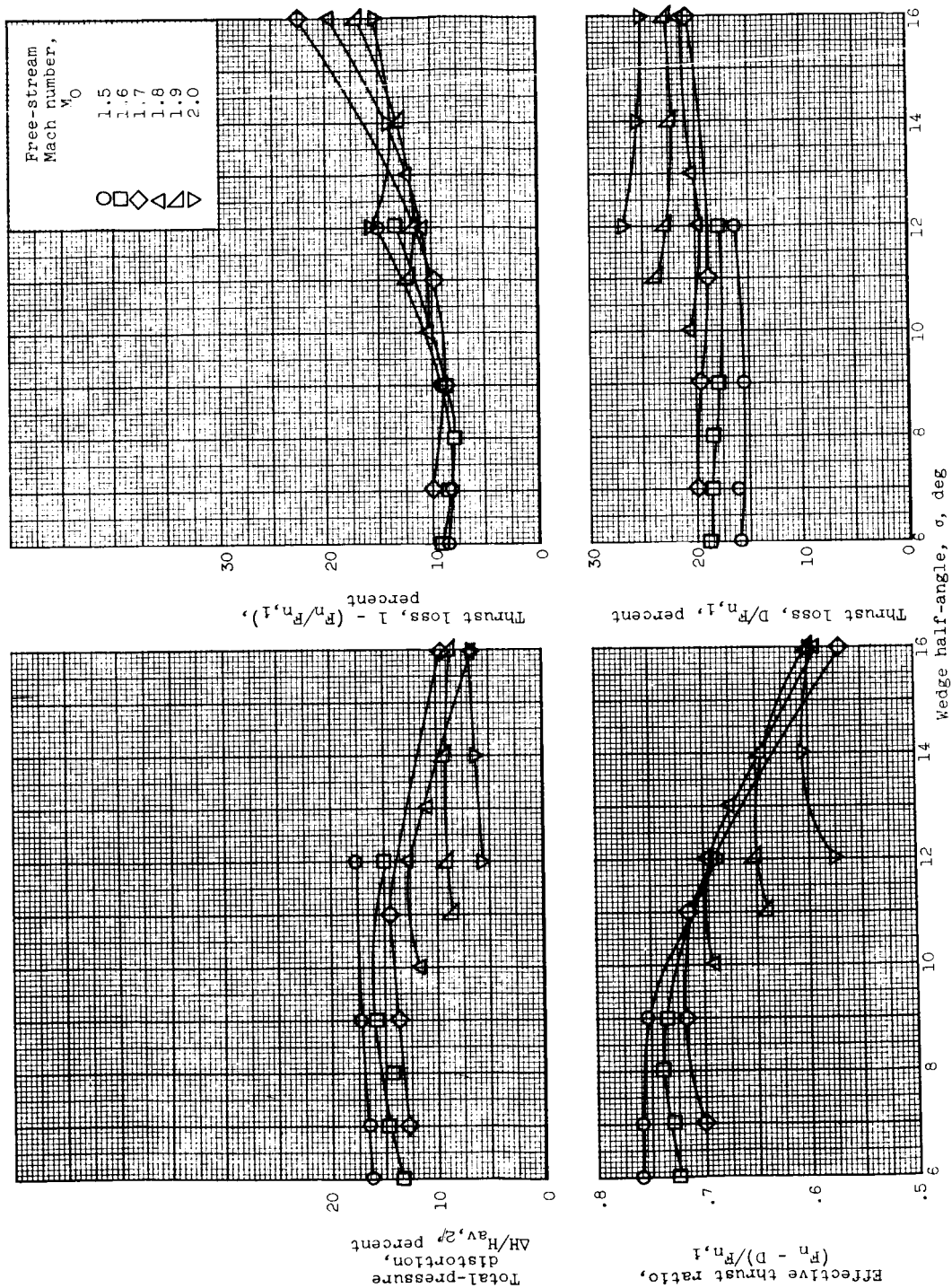
Figure 11. - Effect of porous-wedge angle at engine matching conditions on effective thrust ratio, percentage of thrust loss, and total-pressure distortion for $S_c 5.0E_l$ inlet. Altitude, 35,000 feet.
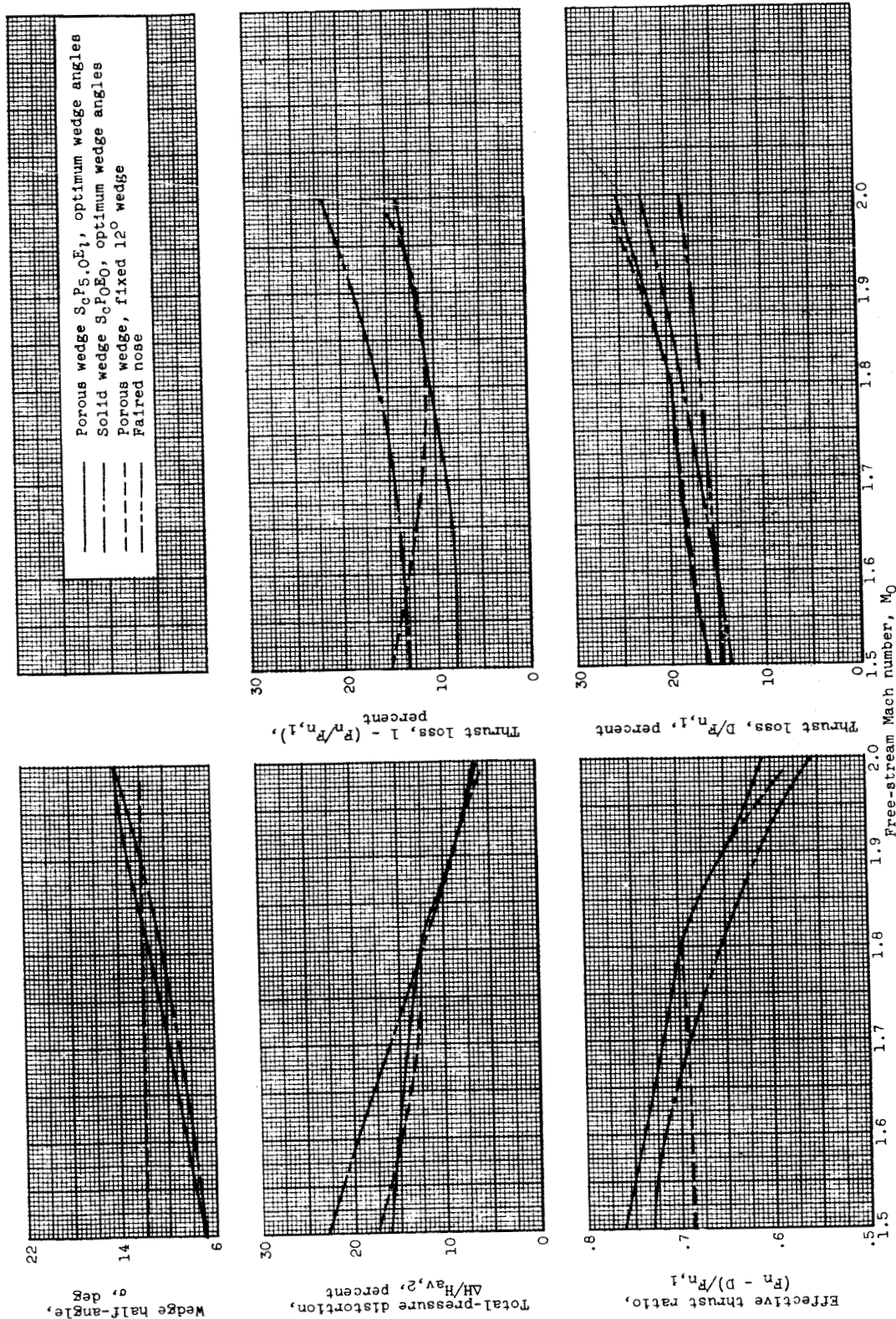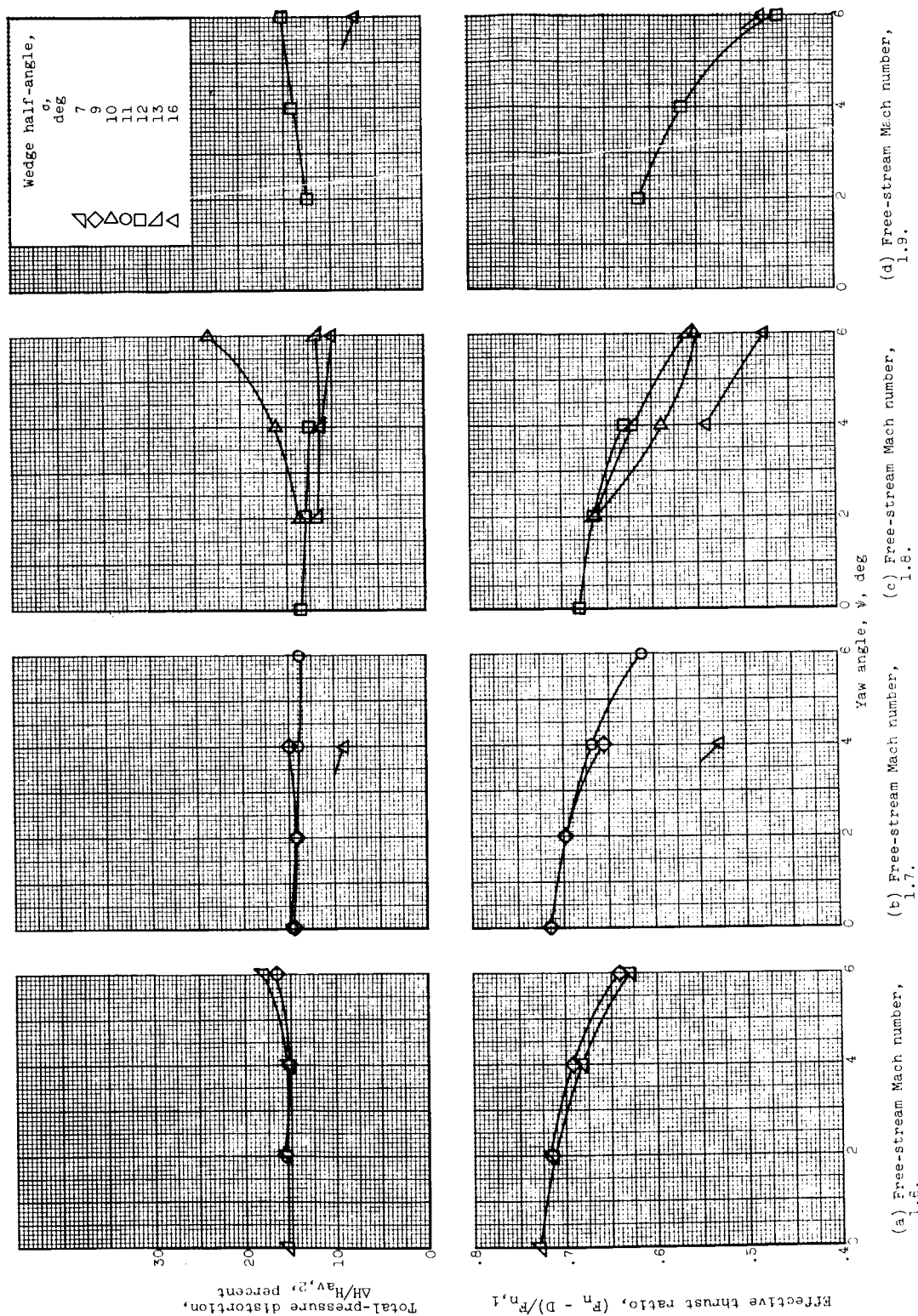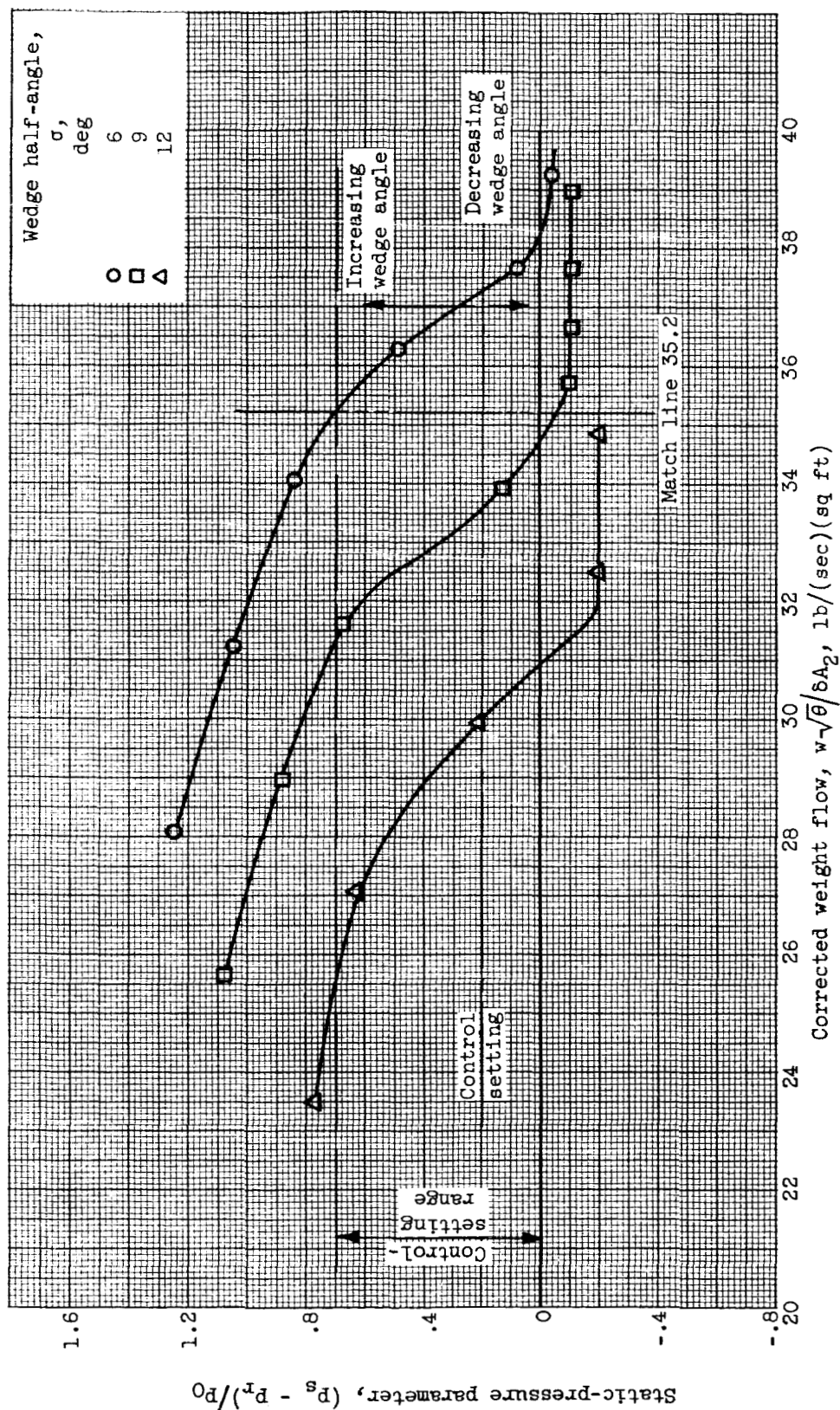
DE █████ SIFIED

Figure 12. - Inlet performance comparison at engine matching conditions. Angle of attack, 2°; altitude, 35,000 feet.

Wedge half-angle,
σ,
deg
7
9
10
11
12
13
16

Total-pressure distortion,
ΔH/H$_{av,2}$, percent

Effective thrust ratio, (F$_n$ – D)/F$_{n,1}$

Yaw angle, ψ, deg

(a) Free-stream Mach number,
1.6.

(b) Free-stream Mach number,
1.7.

(c) Free-stream Mach number,
1.8.

(d) Free-stream Mach number,
1.9.

Figure 23. – Effect of yaw angle on effective thrust ratio and total-pressure distortion at engine matching conditions for S.P5.0E$_l$ inlet.
Altitude, 35,000 feet.
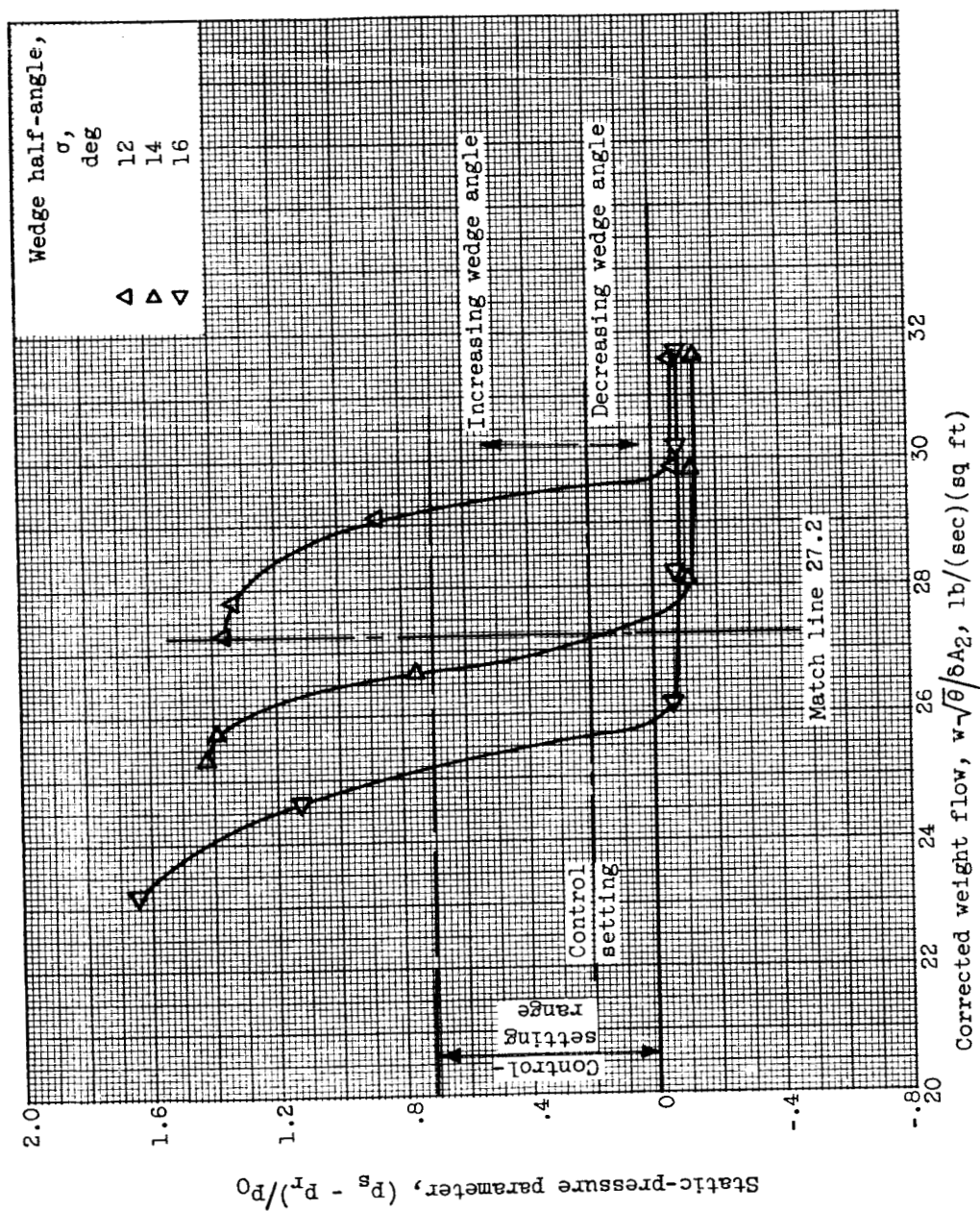
(a) Free-stream Mach number, 1.5.

Figure 14. - Control signal from static-pressure orifices of porous wedge. Angle of attack, 2°.
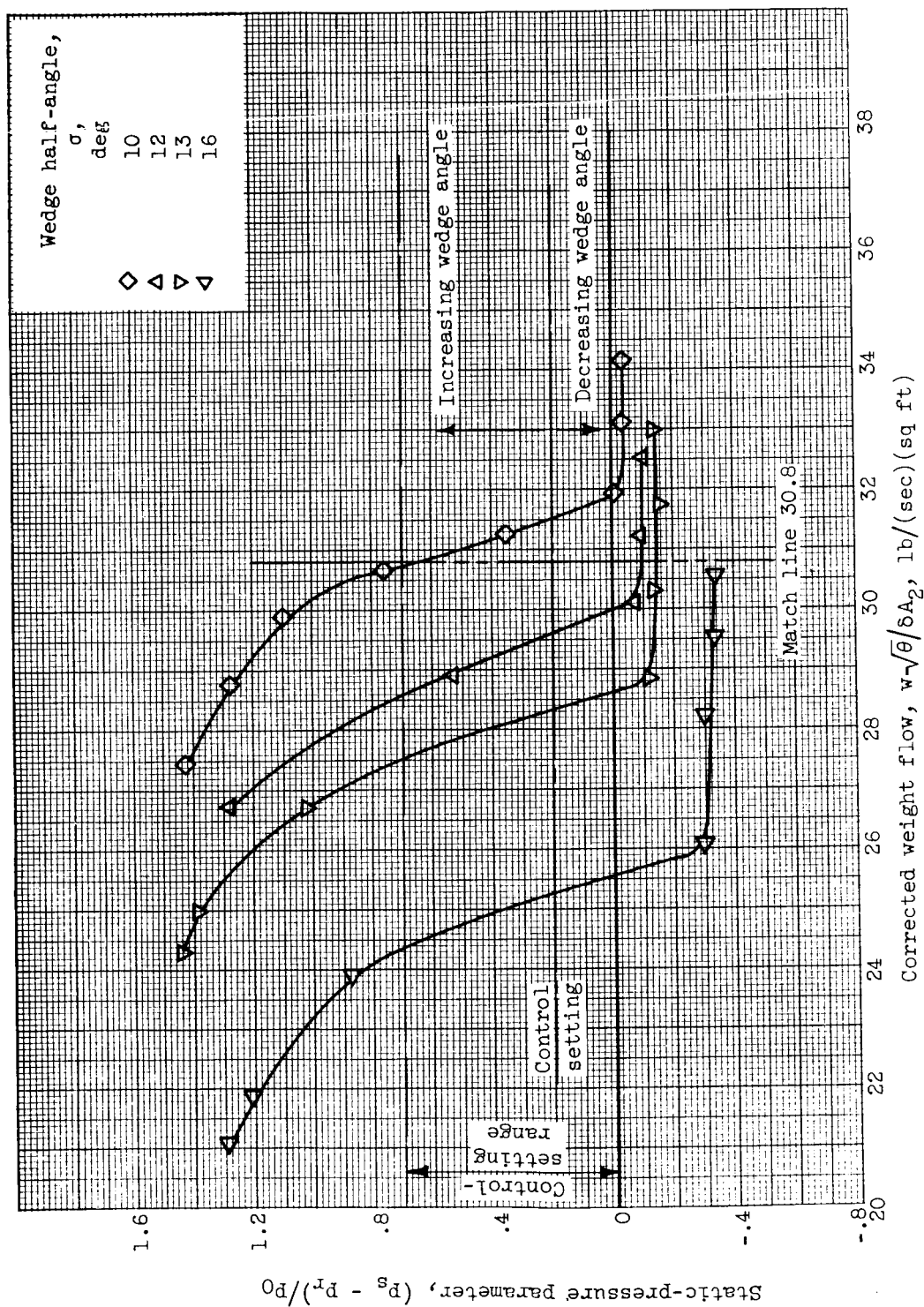
Figure 14. - Continued. Control signal from static-pressure orifices of porous wedge. Angle of attack, 2°.

(c) Free-stream Mach number, 2.0.

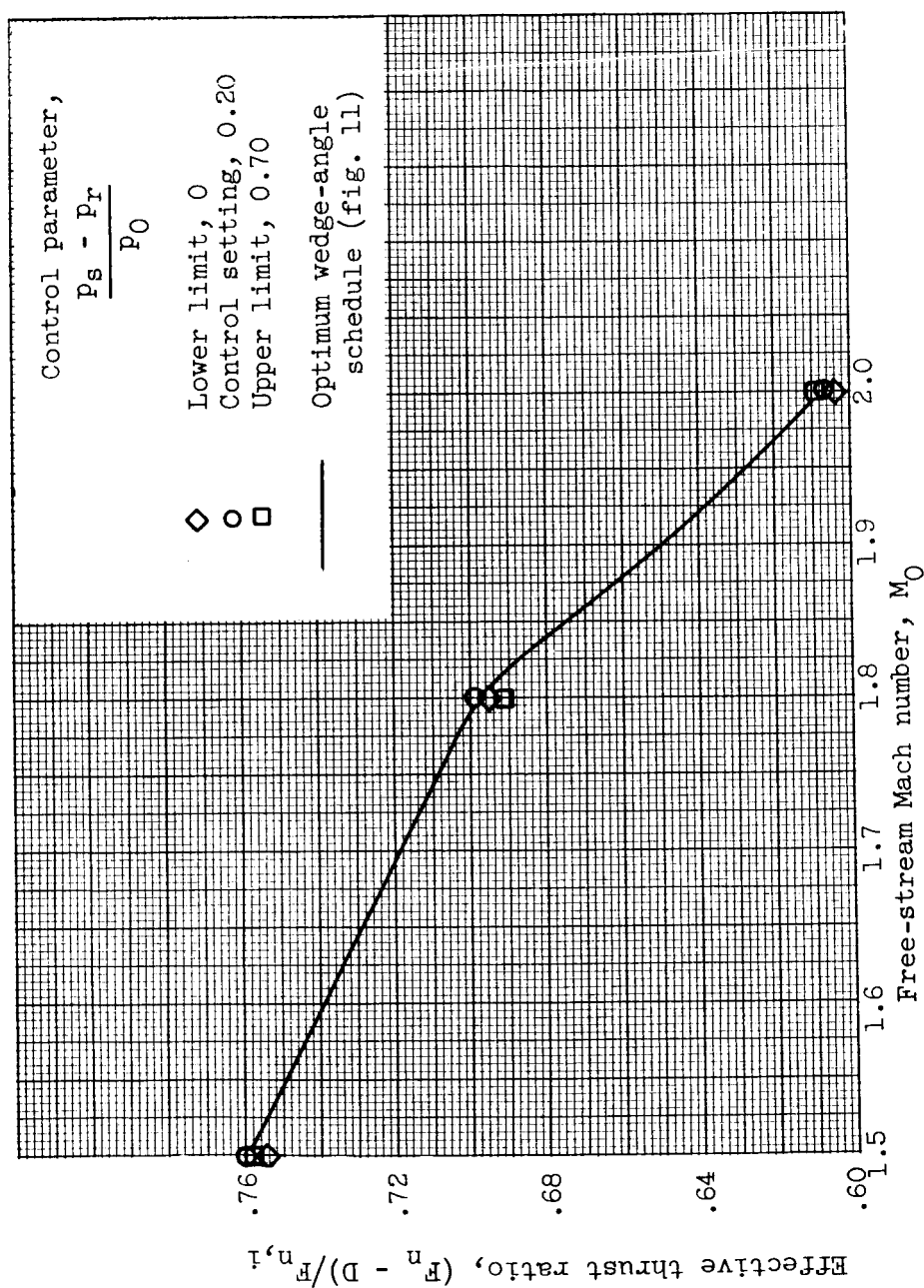Figure 14. - Concluded. Control signal from static-pressure orifices of porous wedge. Angle of attack, 2°.

Figure 15. - Estimated inlet performance using a normal-shock sensing control to vary wedge angle for $S_cP5.0E7$ inlet. Angle of attack, 2°.